

1 **Reconstructing past variations in environmental conditions and paleoproductivity**
2 **over the last ~8000 years off north-central Chile (30° S)**

3
4 Práxedes Muñoz^{1,2}, Lorena Rebolledo^{3,4}, Laurent Dezileau⁵, Antonio Maldonado^{2,6},
5 Christoph Mayr^{7,8}, Paola Cárdenas^{5,9}, Carina B. Lange^{4,10,11}, Katherine Lalangui¹⁰,
6 Gloria Sanchez¹², Marco Salamanca¹⁰, Karen Araya^{1,13}, Ignacio Jara², Gabriel Vargas¹⁴,
7 Marcel Ramos^{1,2}

Comentario [A1]: It should say 4

Comentario [A2]: It should say 9

Comentario [A3]: It should say Easton

8
9 ¹Departamento de Biología Marina, Universidad Católica del Norte, Larrondo 1281,
10 Coquimbo, Chile.

11 ²Centro de Estudios Avanzados en Zonas Áridas (CEAZA), Coquimbo-La Serena,
12 Chile.

13 ³Departamento Científico, Instituto Antártico Chileno, Punta Arenas, Chile

14 ⁴Centro FONDAF de Investigación Dinámica de Ecosistemas Marinos de Altas
15 Latitudes (IDEAL), Universidad Austral de Chile, Campus Isla Teja, Valdivia, Chile.

16 ⁵Normandie University, UNICAEN, UNIROUEN, CNRS, M2C, 14000 Caen, France.

17 ⁶Instituto de Investigación Multidisciplinario en Ciencia y Tecnología, Universidad de
18 La Serena, La Serena, Chile.

19 ⁷Institut für Geographie, FAU Erlangen-Nürnberg, 91058 Erlangen, Germany.

20 ⁸Department of Earth and Environmental Sciences & GeoBio-Center, LMU Munich,
21 80333 Munich.

22 ⁹Programa Magister en Oceanografía, Universidad de Concepción, casilla 160C,
23 Concepción, Chile.

24 ¹⁰Departamento de Oceanografía, Facultad de Ciencias Naturales y Oceanográficas,
25 Universidad de Concepción, Casilla 160C, Concepción, Chile.

26 ¹¹Centro de Investigación Oceanográfica COPAS Sur-Austral, Universidad de
27 Concepción, Casilla 160C, Concepción, Chile.

28 ¹²Universidad de Magallanes, Punta Arenas, Chile.

29 ¹³Laboratoire Géosciences Montpellier (GM), Université de Montpellier, 34095
30 Montpellier Cedex 05, France.

31 ¹⁴Departamento de Geología, Universidad de Chile, Santiago, Chile.

32

33 *Correspondence to:* Práxedes Muñoz (praxedes@ucn.cl)

34

Comentario [A4]: It should say:
Planta de Alimentos Pargua, AquaChile,
Puerto Montt, Chile

35 **Abstract**

36

37 The aim of this project was to establish past variations in the main oceanographic and
38 climatic features of a transitional semi-arid ecosystem in the north-central Chilean coast.
39 We analyzed recent sedimentary records retrieved from two bays, Guanaqueros and
40 Tongoy (30° S), for geochemical and biological analyses, including the following:
41 sensitive redox trace elements, biogenic opal, total organic carbon (TOC), diatoms, and
42 stable isotopes of organic carbon and nitrogen. Three remarkable periods were
43 established with different environmental conditions and productivities: (1) > cal BP
44 6600, (2) cal BP 4500–1800, and (3) cal BP 140 to the present (CE 2015). The first
45 period was characterized by a remarkably higher productivity (higher diatom
46 abundances and opal) in which large fluxes of organic compounds were also inferred
47 from the accumulation of elements, such as Ba, Ca, Ni, Cd, and P in the sediments.
48 Meanwhile, significantly reduced conditions at the bottom of the bays were suggested
49 based on the large accumulation of Mo, Re, and U, showing a peak at cal BP 6600 when
50 sulfidic conditions could have been present. According to the pollen moisture index,
51 this was also identified as the driest interval. These conditions should be associated with
52 an intensification of the Southern Pacific Subtropical Anticyclone and stronger
53 southerly western winds, emulating the La Niña-like conditions, as has been described
54 for the SE Pacific during the early Holocene and part of the mid-Holocene. During most
55 of the second period, lower productivity was observed; however, a small increase was
56 identified between Cal BP 3400 and 4000, although lower amounts of diatom (valves g⁻¹)
57 and nutrient-type metal accumulations were evident. Anoxic conditions at the bottom
58 of the bays changed to an almost stable sub-oxic condition during this time interval. The
59 third period was marked by intense oxygenation after cal BP 1800, as observed by a
60 drastic change in the accumulation of U, Mo, and Re. This was followed by a return to
61 more reduced conditions over the past two centuries, characterized by a small
62 productivity rise after cal BP ~140, as suggested by the opal accumulations. Overall,
63 lower primary productivity, lower reduced conditions at the bottom, and higher
64 humidity conditions were established after cal BP 6600 to the present. We suggest that
65 the oxygenation might be associated with a weak effect from the oxygen minimum zone
66 over the shelf and intensified El Niño activity, introducing oxygenated waters to the
67 coastal zones through the propagation of equatorial waves and establishment of

68 conditions that reduced the primary productivity from the mid-Holocene toward the
69 beginning of the modern era.
70 Keywords: paleoproductivity, paleoredox, trace metals, diatoms, opal, organic carbon,
71 Coquimbo, SE Pacific

72

73 **1. Introduction**

74

75 The mean climatic conditions in the SE Pacific are modulated by the dynamics of the
76 Southern Pacific Subtropical Anticyclone (SPSA) and Humboldt Current System. The
77 coastal wind pattern produced alongshore varies along the SE Pacific, showing lower
78 seasonality between 18°–30° S and producing semi-permanent upwelling (Pizarro et al.,
79 1994; Figueroa and Moffat, 2000). This system is highly affected by the inter-annual
80 variability imposed by the El Niño Southern Oscillation (ENSO), impacting the wind
81 intensity and, therefore, the productivity (Rutlland and Fuenzalida, 1991; Blanco et al.,
82 2002). Other climate patterns demonstrate impacts at longer timescales (inter-annual,
83 decadal, inter-decadal), such as the Pacific Decadal Oscillation (PDO) and the Southern
84 Annular Mode (SAM). These patterns modify the strength and position of the southerly
85 western winds (SWW), producing cold/warm periods that affect mainly winter
86 precipitation during the positive/negative trends of the SAM and lead to intense/weak
87 upwelling (Quintana and Aceituno, 2012; Ancapichún and Garcés-Vargas, 2015). In
88 addition, the orbitally induced variations in the austral insolation influences the extent
89 of the Antarctic sea ice and the Hadley cell, which act as important forces in the
90 latitudinal displacement of the Inter-tropical Convergence Zone (ITCZ; Kaiser et al.,
91 2008, and references therein). These fluctuations produce humid and arid conditions
92 along the SE Pacific where the intensity of the wind remains the key factor in the
93 upwelling strength and, therefore, the supply of nutrients to the photic zone, all of which
94 are required for the development of the primary productivity.

95 Off Coquimbo (30° S), there is normally semi-permanent and intense upwelling forced
96 by local winds, strongly influenced by topographic features (Figueroa and Moffat,
97 2000) and ENSO variability (Schaffer et al., 1997; Escribano et al., 2004). During El
98 Niño, the intensities of the mean winds alongshore are reduced (conversely, during La
99 Niña) (Rahn and Garreaud, 2013), impacting the upper circulation of the ocean and
100 affecting the oxygenation of the water column and strength of the upwelling. The high
101 productivity that takes place close to the coast during normal periods (Escribano et al.,

Comentario [A5]: It should say Rutllant

Comentario [A6]: It should say:
Shaffer et al., 1999

102 2004 and references therein) maintains a zone of low dissolved oxygen content,
103 reinforcing the oxygen minimum zone (OMZ; Helly and Levin, 2004, Ulloa et al.,
104 2012); however, the opposite occurs during El Niño, in which oxygenated waters enter
105 the coastal zone provided by the narrow continental shelf (Helly and Levin, 2004). This
106 changes the normal suboxic conditions at the bottom, normal composition of
107 macrofauna, and related geochemical characteristics of the sediments, with implications
108 that persist for several years after the event (Gutiérrez et al., 2006; Sellanes et al., 2007).
109 These changes in primary productivity and oxygenation at the bottom can be observed
110 in the sedimentary records that respond to the amount of organic carbon that has settled
111 on the surface sediments under different oceanographic and climatic conditions. The
112 diagenetic reactions during organic matter remineralization produce the enrichment or
113 depletion of trace elements, which reflects the amount of settled organic matter but also
114 reinforces the low oxygen conditions imposed by the OMZ, all of which promotes the
115 enrichment or depletion of trace elements (Tribovillard, 2006). Their variability in
116 sedimentary records has been extensively used to establish temporary changes in
117 primary productivity and changes in the oxygenation at the bottom (Nameroff et al.,
118 2002; Zheng et al., 2002; McManus et al., 2006; Siebert et al., 2003).
119 North-central Chile is a semi-arid zone that does not receive large fluvial contributions,
120 except during abnormal periods such as in El Niño years, during which higher runoff
121 has been recorded in austral winter (Valle-204; Levinson et al., 2000; Montecinos and
122 Aceituno, 2003; Garreaud et al., 2009). Under this scenario, marine sediments are often
123 highly influenced by primary production in the water column and terrestrial runoff;
124 therefore, sedimentary records can reveal the past variability in primary production and
125 oceanographic conditions over the shelf, which ultimately respond to the major
126 atmospheric patterns in the region. We considered that redox trace elements off
127 Coquimbo (30° S) respond to changes in the local hypoxia (U, Mo, and Re); in addition,
128 the nutrient-type elements are assumed to have followed the organic flux variability of
129 the sediments (Ba, Ni Cu), according to the interannual and interdecadal variability
130 described for the climatic and oceanographic settings in the region. Similarly, we
131 measured Ca, K, and Pb to assess the terrigenous inputs from runoff and aeolian
132 transportation, which is also impacted by Fe and Mn (Calvert and Pedersen, 2007). Ca
133 accumulation depends, in turn, on carbonate productivity and dissolution, and has also
134 been used as a paleoproductivity proxy (Paytan, 2008; Govin et al., 2012). We
135 determined the enrichment/depletion of elements to establish the primary prevailing

136 environmental conditions during the sedimentation of particulate matter (Böning et al.,
137 2009). In addition, we considered the diatom assemblages with biogenic opal as a
138 measurement of siliceous export production, total organic carbon (TOC), and stable
139 isotopes to identify variations in the organic fluxes to the bottom. Moreover, pollen
140 grains were used to identify environmental conditions based on the climate relationship
141 of the main vegetation formations in north-central Chile. Based on our records we were
142 able to identify wet/dry intervals, periods with high/low organic fluxes to the sediments,
143 which are related to changes in primary production, and changes in the redox conditions
144 at the bottom, which in turn, have been associated with the main climatic conditions
145 described for the Holocene in this region.

146

147 **2. Study area**

148 The Coquimbo area (29–30 °S), in the southern limit of the north-central Chilean
149 continental margin, constitutes a border area between the most arid zones of northern
150 Chile (Atacama Desert) and the more mesic Mediterranean climate in central Chile
151 (Montecinos et al., 2016). Here, the shelf is narrow, and several small bays trace the
152 coast line.

153 The Tongoy and Guanaqueros bays are located in the southern edge of a broad
154 embayment between small islands to the north (29 °S; Choros, Damas, and Chañaral)
155 and Lengua de Vaca Point to the south (30 °S) (Fig. 1), protected from southerly winds
156 that are predominant in the region. Tongoy Bay is a narrow marine basin (10 km at its
157 maximum width) with a maximum depth of approximately 100 m. To the northeast lies
158 Guanaqueros Bay, a smaller and shallower basin. High wind events are evenly
159 distributed throughout the year and promote an important upwelling center at Lengua de
160 Vaca Point, resulting in the accumulation of high biomass along a narrow coastal area
161 (Moraga-Opazo et al., 2011; Rahn and Garreaud, 2013) that reach concentrations of
162 approximately 20 mg m⁻³ (Torres and Ampuero, 2009). In the shallow waters of Tongoy
163 Bay, the high primary productivity results in high TOC in the water column, allowing
164 for the deposition of fine material to the bottom; TOC rises concurrently with periods of
165 low oxygen (Fig. 2; Muñoz et al., unpublished data). Recent oceanographic studies
166 indicate that low dissolved oxygen water intrusions from the shelf (Fig. 3) seem to be
167 related to lower sea levels, resulting from annual local wind cycles at a regional meso-
168 scale (Gallardo et al., 2017). Oceanographic time series indicate that transition times
169 develop in short periods due to changes in the direction and intensity of the winds along

170 the coast, with strong seasonality (<http://www.cdom.cl/boyas-oceanograficas/boya->
171 tongoy). The spatial and temporal variability of these processes is still under study. In
172 addition, oceanic variability along the western coast of South America is influenced by
173 equatorial Kelvin waves on a variety of timescales, from intra-seasonal (Shaffer et al.,
174 1997) and seasonal (Pizarro et al., 2002; Ramos et al., 2006), to inter-annual (Pizarro et
175 al., 2002; Ramos et al., 2008).

176 Sedimentological studies are scarce with regard to the north-central shelf of Chile. A
177 few technical reports indicate that sediments between 27° S and 30° S are composed of
178 very fine sand and silt with relatively low organic carbon content (< 3 and ~5%), except
179 in very limited coastal areas where organic material accounts for approximately 16% of
180 the total material (Muñoz, unpublished data; FIP2005-61 Report, www.fip.cl). Coastal
181 weathering is the main source of continental input owing to scarce river flows and little
182 rainfall in the zone (0.5–80 mm y⁻¹; Montecinos et al., 2016, Fig. 1). Freshwater
183 discharges are represented by creeks, which receive the drainage of the coastal range
184 forming wetland areas in the coast and even small estuaries, such as Pachingo, located
185 south of Tongoy (Fig. 1). These basins cover ~300 and 487 km², respectively. The water
186 volume in the estuaries is maintained by the influx of seawater mixed with the
187 groundwater supply. Normally, a surface flux to the sea is observed. Freshwater
188 discharges only occur through dry creeks that drain water during high rainfall periods in
189 the coastal zone (Dirección General de Aguas, 2011).

190

191 **3. Materials and methods**

192 **3.1. Sampling**

193 Sediment cores were retrieved from two bays in the Coquimbo region: Bahía
194 Guanaqueros (core BGGC5; 30° 09' S, 71° 26' W; 89 m water depth) and Bahía Tongoy
195 (core BTGC8; 30° 14' S, 71° 36' W; 85 m water depth) (Fig. 1), using a gravity corer
196 (KC-Denmark) during May 2015, onboard the L/C Stella Maris II owned by the
197 Universidad Católica del Norte. The length of the cores was 126 cm for BGGC5 and 98
198 cm for BTGC8.

199 Subsequently, the cores were sliced into 1 cm sections, and subsamples were separated
200 for grain size measurements and determination of magnetic susceptibility, trace element
201 and biogenic opal concentrations, C and N stable isotope signatures ($\delta^{13}\text{C}$, $\delta^{15}\text{N}$), and
202 TOC content. The samples first were kept frozen (–20° C) and then freeze-dried before
203 laboratory analyses.

204

205 **3.2. Geochronology (^{210}Pb and ^{14}C)**

206 A geochronology was established combining ages estimated from $^{210}\text{Pb}_{\text{xs}}$ activities
207 suitable for the last 200 years and radiocarbon measurements at selected depths for
208 older ages. The quantification of ^{210}Pb activities was performed through the alpha
209 spectrometry of its daughter ^{210}Po following the procedure of Flynn (1968). The
210 (unsupported) activities of $^{210}\text{Pb}_{\text{xs}}$ were determined as the difference between the ^{210}Pb
211 and ^{226}Ra activities measured in some intervals of the sediment column. Meanwhile,
212 ^{226}Ra was measured by gamma spectrometry at the Laboratoire Géosciences of the
213 Université de Montpellier (France). Standard deviations (SD) of the ^{210}Pb inventories
214 were estimated by propagation of the counting uncertainties (Bevington and Robinson,
215 1992) (Table S1, supplementary data). The ages were based on the Constant Rate of
216 Supply Model (CRS, Appleby and Oldfield, 1978).

217 Radiocarbon measurements were performed on a mix of planktonic foraminifer species
218 in core BGGC5, whereas the benthic foraminifer species *Bolivina plicata* was selected
219 for core BTGC8 (Table 1). The samples were submitted to the National Ocean Sciences
220 AMS Facility (NOSAMS) of the Woods Hole Oceanographic Institution (WHOI). The
221 timescale was obtained from $^{210}\text{Pb}_{\text{xs}}$ and ^{14}C measurements and from Bacon age–depth
222 modeling open source software (Blaauw and Christen, 2011), considering the Marine
223 curve ^{13}C (Reimer et al., 2013) (Fig. 4) and a reservoir deviation from the global mean
224 reservoir age of 441 ± 35 y. This was estimated subtracting the ^{14}C age value
225 corresponding at the historical dates 1828 AD and 1908 AD (499 ± 24 and 448 ± 23 ^{14}C
226 y, respectively, Reimer et al., 2013) from the apparent ^{14}C age of the foraminifers
227 measured at depths of 5 and 10 cm for cores BTGC8 and BGGC5, respectively
228 (Sabatier et al., 2010; Table 2).

229

230 **3.3. Geophysical characterization**

231 The magnetic susceptibility ($\text{SI} \times 10^{-8}$) was measured with a Bartington Susceptibility
232 Meter MS2E surface scanning sensor at the Sedimentology Laboratory at Centro Eula,
233 Universidad de Concepción. Mean values from three measurements were calculated for
234 each sample.

235 The grain size was determined using a Mastersizer 2000 laser particle analyzer (Hydro
236 2000–G, Malvern) in the Sedimentology Laboratory at Universidad de Chile. Skewness,

237 sorting, and kurtosis were evaluated using the GRADISTAT statistical software (Blott
238 and Pye, 2001), which includes all particle size spectra.

239

240 **3.4. Chemical analysis**

241 Trace element analyses were performed via inductively coupled plasma-mass
242 spectrometry (ICP-MS) using an Agilent 7700x at Université de Montpellier (OSU
243 OREME/AETE regional facilities). The analysis considered reference materials (UBN,
244 BEN, and MAG1) that had an accuracy higher than $\pm 5\%$; the analytical precisions were
245 between 1% and 3%. Internal standardizations with In and Bi were used to deconvolve
246 the mass-dependent sensitivity variations of both matrix and instrumental origin
247 occurring during the course of an analytical session. The analytical precisions attained
248 were between 1% and 3%.

249 The element concentrations were normalized using Al due to its conservative behavior
250 that allows assessing the relative enrichment/depletion of elements and evaluating the
251 crustal contribution for each element (Calvert and Pedersen, 2007). The authigenic
252 enrichment factor (EF) was estimated as: $EF = (Me/Al)_{\text{sample}} / (Me/Al)_{\text{detrital}}$, where
253 $(Me/Al)_{\text{sample}}$ is the bulk sample metal (Me) concentration normalized to the Al content,
254 and the denomination “detrital” indicates a lithogenic background (Böning et al., 2009).
255 Detrital ($[Me]_{\text{detrital}}$ and $[Al]_{\text{detrital}}$) concentrations were established considering the local
256 metal abundance, which is more accurate than using mean Earth crust values (Van der
257 Weijden, 2002). We used average element concentrations on surface sediments (0–3
258 cm) of the Pachingo wetland (Table 3).

259 TOC and stable isotope ($\delta^{15}\text{N}$ and $\delta^{13}\text{C}$) analyses were performed at the Institut für
260 Geographie, Friedrich Alexander Universität (FAU) Erlangen-Nürnberg, Germany
261 using a Carlo Erba elemental analyzer NC2500 and an isotope–ratio–mass spectrometer
262 (Delta Plus, Thermo-Finnigan) for isotopic analysis. Stable isotope ratios were reported
263 in the δ notation as the deviation relative to international standards (Vienna Pee Dee
264 Belemnite for $\delta^{13}\text{C}$ and atmospheric N_2 for $\delta^{15}\text{N}$); thus, $\delta^{13}\text{C}$ or $\delta^{15}\text{N} = [(R_{\text{sample}}/R_{\text{standard}}) - 1] \times 10^3$, where R is $^{13}\text{C}/^{12}\text{C}$ or $^{15}\text{N}/^{14}\text{N}$, respectively. The typical precision
265 of the analyses was $\pm 0.1\%$ for $\delta^{15}\text{N}$ and $\delta^{13}\text{C}$.

267 Biogenic opal was estimated following the procedure described by Mortlock and
268 Froelich (1989). The analysis was performed by molybdate-blue spectrophotometry
269 (Hansen and Koroleff, 1999), conducted at the laboratories of Marine Organic

270 Geochemistry and Paleoceanography, University of Concepción, Chile. Values for
271 biogenic opal were expressed by multiplying the Si (%) by 2.4 (Mortlock and Froelich,
272 1989). The analytical precision was $\pm 0.5\%$. Accumulation rates were determined based
273 on the sediment mass accumulation rates and amount of opal for each core section in %.

274

275 **3.5. Microfossils analyses**

276 Qualitative abundances of siliceous microfossils were determined for every 1 cm
277 following the Ocean Drilling Program (ODP) protocol, described by Mazzullo and
278 Graham (1988). This information was used to select sections every 4, 8, and 12 cm for
279 BGGC5 and every 6 cm for BTGC8, to determine quantitative abundances of
280 microfossils (diatoms, silicoflagellates, sponge spicules, crysophyts, and phytoliths).
281 Roughly 0.5 g of freeze-dried sediment was treated according to Schrader and Gersonde
282 (1978) for siliceous microfossils. They were identified and counted under an Olympus
283 CX31 microscope with phase contrast, in which 1/5 of the slides were counted at 400X
284 for siliceous microfossils and one transect at 1000X was counted for *Chaetoceros*
285 resting spores (*Ch. RS*). Two slides per sample were counted with an estimated
286 counting error of 15%. Total diatom abundances are given in valves g^{-1} of dry
287 sediments.

288 Pollen analysis was conducted following the standard pollen extraction methodology
289 (Faegri and Iversen, 1989). The identification was conducted under a stereomicroscope,
290 with the assistance of the Heusser (1973) pollen catalog. A total of 100–250 terrestrial
291 pollen grains were counted in each sample. The pollen percentage for each taxon was
292 calculated from the total sum of terrestrial pollen (excluding aquatic taxa and fern
293 spores). Pollen percentage diagrams and zonation were generated using the Tilia
294 software (Grimm, 1987).

295 We further summarize pollen-based precipitation trends by calculating a pollen moisture
296 index (PMI), which is defined as the normalized ratio between Euphorbiaceae (wet
297 coastal scrubland) and Chenopodiaceae (arid scrubland). Thus, a positive (negative)
298 value for this index point corresponds to relatively wetter (drier) conditions.

299

300 **4. Results**

301 **4.1. Geochronology**

302 The activity of $^{210}\text{Pb}_{\text{xs}}$ (unsupported) was obtained from the surface to a depth of 8 cm
303 in the two cores, with an age of ~AD 1860 at 8 cm in both (Table S1). Greater surface

304 activities were obtained for core BGGC5 (13.48 ± 0.41 dpm g⁻¹) than core BTGC8 (5.80
305 ± 0.19 dpm g⁻¹), showing an exponential decay with depth (Fig. 4). A recent
306 sedimentation rate of 0.11 ± 0.01 cm y⁻¹ was estimated.

307 The age–depth model provided a maximum age of cal BP 7990 for core BGGC5 and cal
308 BP 8012 for core BTGC8 (Fig. 4). A mean sedimentation rate of 0.026 ± 0.012 cm y⁻¹
309 was estimated for core BGGC5, with a period of relatively low values (< 0.01 cm y⁻¹)
310 between cal BP 240 and 1500 and between cal BP ~5000 and 6400. This variation in the
311 accumulation rates occurred over a few centimeters (5 and 7 cm, respectively); thus, this
312 rapid decrease was considered as a hiatus in the age–depth modeling. The model
313 estimates the accumulation rates before and after the hiatus not auto-correlated,
314 obtaining variable sedimentation rates which are more accurate to the sedimentation
315 process. We could not resolve the length and time of hiatuses; we assumed an elapsed-
316 time of 1400 years based on the difference between the radiocarbon ages before and
317 after the hiatus and a mid-depth corresponding to those gaps. Although we did not have
318 stratigraphic evidence of these discontinuities in the sediment core, we believe that the
319 assumptions considered allowed the development of reasonable age–depth models.

320 Nevertheless, the interpretations of the proxy records were taken with caution in these
321 age ranges. For BTGC8, mean sedimentation rates were less variable in the entire core
322 at 0.013 ± 0.006 cm y⁻¹. The local reservoir deviation values were close to the global
323 marine reservoir (Table 2) and higher than other estimations along the Chilean margin
324 at shallower depths (146 ± 25 years at < 30 m water depth; Carré et al., 2016; Merino-
325 Campos et al., 2018). Our coring sites are deeper (~90 m water depth) and influenced by
326 upwelling water from Lengua de Vaca Point, which could explain such differences.

327 However, moderate differences were observed between the models using both reservoir
328 values. Thus, our estimations were based on two pre-bomb values established with ²¹⁰Pb
329 measured in sediments and ¹⁴C in foraminifers, used for the age modeling.

330

331 **4.2. Geophysical characterization**

332 Sediments retrieved from the bays showed fine grains within the range of very fine sand
333 to silt in the southern areas. There, grain size distribution was mainly unimodal, very
334 leptokurtic, more sorted, and skewed to fine grain when compared with sediments from
335 the northern areas. Sediment cores obtained from the northern areas were sandy (coarse
336 sand and gravel) with abundant calcareous debris. Longer cores of soft sediment were
337 retrieved at the southernmost areas (BGGC5 and BTGC8, Fig. 1), where the silty

338 component varied between 40% and 60% (Figs. 5a, 5b). The clay component was very
339 low at both cores (< 2%). The sediment's color ranged from very dark grayish brown to
340 dark olive brown (2.5Y 3/3–3/2) in Guanaqueros Bay (BGGC5) and from dark olive
341 gray to olive gray (5Y 3/2–4/2) in Tongoy Bay (BTGC8). Visible macro-remains (snails
342 and fish vertebrae) were found, as well as weak laminations at both cores. The magnetic
343 susceptibility showed higher values close to the surface, up to 127×10^{-8} SI at BGGC5,
344 and lower values (85×10^{-8} SI) at BTGC8. At greater depths, however, the values were
345 very constant, at $5\text{--}8 \times 10^{-8}$ SI at BGGC5 core and $12\text{--}20 \times 10^{-8}$ SI at BTGC8 core. In
346 both cores, susceptibility rose substantially in the last century (Figs. 5a, 5b). Lower bulk
347 densities were estimated at core BGGC5 ($0.7\text{--}0.9 \text{ g cm}^{-3}$), compared with core BTGC8
348 ($> 1 \text{ g cm}^{-3}$) (Figs. 5a, 5b). Consistent with this, the mean grain size amounted to 60–80
349 μm in Guanaqueros Bay (BTGC8), compared with 50–60 μm in Tongoy Bay
350 (BGGC5). Both cores were negatively skewed, with values of -1 to -1.2 at BGGC5,
351 and -1 to -2.5 at BTGC8. Minor increases toward coarser grain size were observed over
352 the past ~ 1000 years, especially in Tongoy Bay (BTGC8). In both cases, grain size
353 distributions were strongly leptokurtic. The Ca/Fe ratio also reduced with time, except
354 at core BTGC8 where it was only observed during the last ~ 2000 years.

355

356 4.3. Biogenic components

357 4.3.1. Siliceous microfossils and biogenic opal

358 The total diatom abundance fluctuated between 5.52×10^5 and 4.48×10^7 valves g^{-1} at
359 core BGGC5. This abundance showed good correlation with biogenic opal content at
360 BGGC5 ($R^2 = 0.52$, $P < 0.5$), with values increasing from 72 cm to the bottom of the
361 core, corresponding to cal BP 4900, and reaching their highest values before cal BP
362 6600. The opal percentage exhibited a maximum before cal BP 4900 (mode = 15.8%).
363 In contrast, the diatom abundance and biogenic opal were much lower at core BTGC8
364 ($< 2 \times 10^5$ valves g^{-1} and $< 3\%$, respectively). Here, the siliceous assemblage was almost
365 completely conformed by *Ch. RS* (Fig. 6).

366 A total of 135 and 8 diatom taxa were identified in cores BGGC5 and BTGC8,
367 respectively, whereby core BTGC8 registered very low diatom abundances. In general,
368 diatoms were the most important assemblage of siliceous microfossils (96%), followed
369 by sponge spicules (3%). The contributions of phytoliths and chrysophyte cysts were
370 less than 2% at core BGGC5. *Ch RS* was dominant in the diatom assemblage ($\sim 90\%$;
371 Fig. 6) and included the species *C. radicans*, *C. cinctus*, *C. constrictus*, *C. vanheurckii*,

Comentario [A7]: It should say formed

372 *C. coronatus*, *C. diadema*, and *C. debilis*. Other recorded upwelling group species
373 (mainly at core BGGC5) were *Skeletonema japonicum* and *Thalassionema nitzschioides*
374 var. *nitzschioides* (Table S2). Other species range from 0.3% to 6% of the total
375 assemblage.

376

377 **4.3.2. TOC and stable isotope distribution**

378 Consistent with opal and diatoms, core BGGC5 showed higher values of TOC
379 (between 2% and 5%) compared with less than ~1.5% at core BTGC8 (Figs. 5a, 5b).
380 Furthermore, $\delta^{13}\text{C}$ was slightly higher at core BTGC8 (-20‰ to -21‰) compared with
381 core BGGC5 (-21‰ to -22‰). The former also shows slightly higher values of $\delta^{15}\text{N}$
382 from the deeper sections to the surface of the core (< 7‰ to > 10‰). This increase
383 was less evident at core BGGC5, with values of ~9‰ at depth to > 10‰ at the surface
384 (Figs. 5a, 5b). The reduced TOC content was related to the slightly higher $\delta^{13}\text{C}$ values
385 (approximately -20‰) in both cores.

386

387 **4.3.3. Pollen record**

388 Initial surveys at core BTGC8 (Tongoy Bay) revealed extremely low pollen
389 abundances, which hampered further palynology work. A comprehensive pollen
390 analysis was conducted only for core BGGC5 (Guañeros Bay). The pollen record
391 of core BGGC5 consisted of 29 samples shown in Fig. 7. The record was divided into
392 five general zones following visual observations of changes in the main pollen types
393 and was also assisted by CONISS cluster analysis.

394 Zone BG-1 (cal BP 7990–7600): This zone is dominated by the herbaceous taxa
395 Chenopodiaceae, *Leucheria*-type, Asteraceae subfamily (subf.) Asteroideae, and
396 Apiaceae with overall high values for the wetland genus *Typha* spp.

397 Zone BG-2 (cal BP 7600–6700): This zone is also dominated by Chenopodiaceae,
398 *Leucheria*-type, and Asteraceae subf. Asteroideae. In addition, other non-arboreal
399 elements, such as *Ambrosia*-type, Poaceae, Brassicaceae, and *Chorizanthe* spp.,
400 increase considerably.

401 Zone BG-3 (cal BP 6700–3500): This zone is marked by a steady decline in
402 Chenopodiaceae and *Leucheria*-type and by the increase in several other herbaceous
403 elements, such as Euphorbiaceae, *Baccharis*-type, and Brassicaceae.

404 Zone BG-4 (cal BP 3500–50): This zone is mostly dominated by Ast. subf.
405 Asteroideae and is marked by a decline in Chenopodiaceae and *Leucheria*-type. Other
406 coastal taxa, such as Euphorbiaceae, *Baccharis*-type, Asteraceae subf. Chichorioideae,
407 *Quillaja saponaria*, Brassicaceae, and *Salix* spp., also increase in this zone.
408 Zone BG-5 (cal BP 50–Present): The upper portion of the record is dominated by
409 Asteraceae subf. Asteroideae and Poaceae and is marked by higher amounts of
410 Geraniaceae, Asteraceae subf. Mutisieae, Myrtaceae, and *Q. saponaria*. Additionally,
411 this zone includes introduced pollen types such as *Rumex* spp. and *Pinus* spp. The
412 latter is not shown in Fig. 7 because its abundance was minimal.
413 Overall, the most distinctive trend revealed by core BGGC-5 is a long-term decline in
414 Chenopodiaceae and higher amounts of Euphorbiaceae and Asteraceae subf.
415 Asteroideae. Along with these changes, a further increase of several other types of
416 pollen, representative of the coastal shrub land vegetation, began at approximately cal
417 BP 6700.

418

419 **4.4. Trace element distributions**

420 Trace elements are presented as metal/Al ratios in Figs. 8a and 8b for Guanaqueros
421 (BGGC5) and Tongoy Bays (BTGC8), respectively. The metals that are sensitive to
422 changes in the oxygen concentration (U, Re, Mo), showed an increasing metal/Al ratio
423 from the base of core BGGC5 (cal BP ~7990) up to cal BP 6600. After this peak, these
424 ratios increased slightly toward cal BP 1800, close to the beginning of the recent era,
425 followed by a sharp reduction until present. The exception to this trend was Mo, which
426 reached a maximum value up to cal BP 6600 and then reduced steadily to the present.
427 Similarly, metal ratios at core BTGC8 increase over time; however, the peak was
428 observed at cal BP ~1000 for U and Re and at cal BP 6000 for Mo, with a second
429 minor peak at cal BP 3400. Iron revealed a clear upward trend at cal BP 3500–3800
430 for core BGGC5 and a second peak between cal BP 4500 and 6500, which was not
431 clearly observed at the Tongoy core (BTGC8). Instead, core BTGC8 showed higher
432 values before cal BP 6400. In both cores, Fe increased over the past ~80 years,
433 whereas no clear trend could be established for Mn. In general, metal/Al values were
434 higher at core BGGC5.

435 A second group of elements (metal/Al ratio), including Ca, Ni, Cd, and P (related to
436 primary productivity and organic fluxes), showed a pattern similar to that of Mo/Al of
437 core BGGC5, i.e., increasing values from cal BP ~7990, reaching the highest values

438 near cal BP 6600–7000; afterwards, the values followed a constant reducing trend
439 toward the present. Otherwise, Cu/Al (a nutrient-type element) showed a different
440 pattern, similar to the Fe/Al distribution, with a maximum value at cal BP 3500–3800
441 and a conspicuous upward trend over the past ~80 years. A third group, consisting of
442 Ba and Sr, exhibited a similar pattern but smoother, showing the maximum values
443 before cal BP 6600. At BTGC8 core, a less clear pattern was demonstrated. Ca, Ni,
444 Cd, and P ratios at core BTGC8 showed only slightly decreasing values and very low
445 peak values compared with core BGGC5; however, Ni/Al showed increasing
446 concentrations over the past 80 years, which was not observed at core BGGC5.
447 Metal/Al ratios of Ba and Sr showed no substantial variation in time. In general, all the
448 elemental concentrations were lower in core BTGC8 than in core BGGC5 and
449 presented similar long-term reduction patterns toward the present, except for Cu, Ni,
450 and Fe.

451 The authigenic enrichment expressed as EF values, suggest a large enrichment of
452 nutrient-type elements in a period prior to cal BP 6600, following the trend of the
453 Me/Al ratios, except for Ba and Fe, which did not show authigenic enrichment. The EFs
454 exhibited a sharp decrease in enrichment in recent times after cal BP 90 (Fig. 9).

455

456 **5. Discussion**

457 **5.1. Sedimentary composition of the cores: terrestrial *versus* biogenic inputs**

458 The sediments in the southern zones of the bays are a sink of fine particles transported
459 from the north and the shelf (Figs. 5a, 5b), and respond to water circulation in the
460 Guanaqueros and Coquimbo Bays (Fig. 1) with two counter-rotating gyres moving
461 counterclockwise to the north and clockwise to the south (Valle-Levinson and
462 Moraga, 2006) (Fig. 1). The differences established by the sediment composition of
463 the bays show that the sediments of Guanaqueros Bay better represent the organic
464 carbon flux to the bottom, with higher accumulation rates (mean value: $16 \text{ g m}^{-2} \text{ y}^{-1}$)
465 and higher amounts of siliceous microfossils. Furthermore, is it a better zone than
466 Tongoy for pollen identification (Figs. 5a, 6 and 7). Both areas have sediments
467 composed by winnowed particles and relatively refractory material (C/N: 9–11),
468 which has a slightly lower isotopic composition than the TOC composition in the
469 column water (–18‰, Fig. 2) and is transported by water circulating over the shelf.

470 The isotopic variations in $\delta^{13}\text{C}$ and $\delta^{15}\text{N}$ did not clearly establish differences between
471 the sediments of the two bays; however, minor differences in $\delta^{15}\text{N}$ would indicate a
472 greater influence of the upwelling nutrient supply and OMZ on the shelf, resulting in a
473 $\delta^{15}\text{N}$ of 9–10‰ in the Guanaqueros Bay, values which are slightly higher than that in
474 the Tongoy Bay sediments (Figs. 5a, 5b). This isotopic composition corresponds with
475 that of NO_3^- in the upwelling waters (De Pol-Holz et al., 2007) in the range of those
476 measured at north-central Chile (~11‰; Hebbeln et al., 2000, De Pol-Holz et al.,
477 2007, 2009). This is due to the isotopic fractionation of NO_3^- during nitrate reduction
478 within the OMZ, which leaves remnant NO_3^- enriched in ^{15}N (Sigman et al., 2009;
479 Ganeshram et al., 2000 and references therein). This is particularly relevant because it
480 demonstrates the relevance of OMZ over the shelf sediments off Coquimbo at shallow
481 depths and the influence of the poleward undercurrent from the Perú OMZ (Mollier-
482 Vogel et al., 2012).

Comentario [A8]: It should say 2019

483 At sediment core BTGC8, lower values (< 8‰) measured at greater depths within the
484 core should account for a mix with isotopically lighter terrestrial organic matter
485 (Sweeney and Kaplan, 1980), owing to its proximity to a small permanent wetland in
486 the southern side of Tongoy Bay (Pachingo), the sediments of which have $\delta^{15}\text{N}$ of 2–
487 6‰ (Muñoz et al., data will be published elsewhere). This suggests that the Tongoy
488 sediments contain a greater proportion of continental material compared to
489 Guanaqueros Bay (Fig. 5b).

490 Thus, cores BGGC5 and BTGC8 in the Guanaqueros and Tongoy Bays record the
491 variability in oceanographic conditions; however, in the Tongoy core, the
492 concentration of oceanographic proxies is diluted owing to the input of terrigenous
493 material. This helps to decipher the climatic variability, considering that the main
494 input of clastic material to the area takes place during major flooding events.
495 Additionally, the main circulation of the bay system leads to favorable conditions for
496 the sedimentation and preservation of organic marine proxies in Guanaqueros Bay,
497 making the sedimentary records of these sites complementary.

498

499 **5.2. Temporal variability of primary productivity and the oxygenation of bottoms**

500 Ca, Sr, Cd, and Ni profiles suggest a lower share of organic deposition over time
501 (Figs. 8a, 8b), consistent with the slight reduction in TOC content observed in the

502 sediments (Figs. 5a, 5b) and concomitant with the other elements related to organic
503 fluxes to the bottom and primary productivity. Similarly, the maximum Ba
504 concentrations indicate higher productivity before cal BP 6600. The same is true for
505 Ca, Cd, and Ni, suggesting that the maximum productivity and organic fluxes to the
506 bottom occurred during this period. After this age, the reduction in TOC and other
507 nutrient-type elements (Ni, Sr, Ca, Cd) to the present is consistent with the increase in
508 oxygen at the bay bottom.

509 The slight rise in Ba in the last ~115 years (Fig. 8a) is a response to a less anoxic
510 environment, owing to better preservation within the sediments in less anoxic
511 environments with moderate productivity (Torres et al., 1996; Dymon et al., 1992) as
512 is the case with our study site (Gross Primary Productivity = 0.35 to 2.9 g C m⁻¹d⁻¹;
513 Daneri et al., 2000). This leads to a negative correlation with TOC (-0.59; Table 4),
514 owing to the remobilization of Ba under anoxic conditions before cal BP 6600.
515 Meanwhile, the P distribution showed a trend similar to that of TOC and the other
516 elements related to the organic fluxes to the bottom (Ni, Cd), although with a lower
517 correlation (~0.6). This is consistent with the distributions observed for U, Re, and Mo
518 at core BGGC5, which indicate that anoxic or suboxic conditions were developed
519 from cal BP 7990 to 1800 but were stronger before cal BP 6600 (Figs. 8a, 8b). After
520 this period and to the present, a remarkable reduction in their concentration suggests a
521 more oxygenated bottom environment, concurrent with lower organic fluxes to the
522 sediments. The Re profile shows the influence of suboxic waters not necessarily
523 associated with higher organic matter fluxes to the bottom. Since this element is not
524 scavenged by organic particles, its variability is directly related to oxygen changes
525 (Calvert and Pedersen, 2007, and references therein).

526 Otherwise, the accumulation of P depends on the deposition rate of organic P (dead
527 plankton, bones, and fish scales) on the bottom and is actively remineralized during
528 aerobic or anaerobic bacterial activity. P and TOC showed a declining trend toward
529 the present, suggesting a reduction in flux of organic matter over time, which was also
530 observed for Ni and Cd distributions. Alternatively, the reducing fluxes of organic
531 proxies could be explained by the higher remineralization of organic material settled at
532 the bottom due to higher oxygen availability, as shown by U, Mo, and Re distributions
533 (Figs. 8a, 8b). However, the lower $\delta^{15}\text{N}$, depending on the denitrification process, is

534 similar to that at deeper environments in the zone (De-Pol Holz et al., 2009),
535 suggesting that the influence of the reductive environment of OMZ over the shelf and
536 changes in U, Mo and Re records could depend mainly on the OMZ variability. Thus,
537 the influence of the primary productivity on oxygen consumption at the bottom over
538 time would be secondary in this system, which is considered to be moderated in
539 productivity compared with upwelling centers in north and south Chile.

Comentario [A9]: It should say:
De Pol-Holz

540 Productivity reconstructions were based on the qualitative relative abundances of
541 diatom and sponge spicules, quantitative diatom counts (valves g^{-1}), and biogenic opal
542 content only in core BGGC5, since core BTGC8 registered low valve counts ($< 1\%$ in
543 relative diatom abundance). However, in both cores, diatom assemblages were
544 represented mainly by *Ch. RS*, which are used as upwelling indicators (Abrantes 1988,
545 Vargas et al., 2004). The downcore siliceous productivity based on opal distribution
546 (Figs. 6 and 9) distinguished three main time intervals of higher productivity, which
547 coincided with the ages highlighted by the distribution of the sedimentary proxies
548 noted previously: (1) $> \text{cal BP } 6600$, (2) $\text{cal BP } 4500\text{--}1800$, and (3) $\text{cal BP } \sim 140$ to
549 recent times (CE 2015). Other periods between $\text{cal BP } 6600$ and $\text{cal BP } 4500$ and
550 between $\text{cal BP } 1800$ and $\text{cal BP } 140$ did not experience higher productivities.

551 At first period ($> \text{cal BP } 6600$), the opal accumulation rate was remarkably high,
552 amounting to $\sim 35 \pm 18 \text{ g m}^{-2} \text{ y}^{-1}$ (range: $16\text{--}119 \text{ g m}^{-2} \text{ y}^{-1}$, Fig. 9) when *Chaetoceros*
553 spores were predominant, indicating an intensification in upwelling. During this
554 period, all metal proxies suggest that primary productivity increases before $\text{cal BP } 6600$,
555 owing to the high concentrations and major enrichment of Ni, Ca, and P that
556 occurred in this period, concomitant with higher opal accumulation within the
557 sediments (Fig. 6 and 9). From these elements, Ni is the best indicator of organic
558 sinking flux related with diatom productivity in organic-rich upwelling sediments
559 (Böning et al., 2015), which helps to sustain our statement. In addition, the authigenic
560 enrichments of Cd were very high (> 100 , Fig. 9) resulting in high Cd/U ratios (> 2 ;
561 Fig. 9), indicative for anoxic conditions as this ratio could vary between 0.2 and 2,
562 from suboxic to anoxic environments (Nameroff et al., 2002). The Cd accumulation in
563 this period was higher than that reported for a highly productive zone off Concepción
564 in periods of high organic carbon accumulation in the sediments (~ 5 , Muñoz et al.,
565 2012). Additionally, the high enrichment of Mo (~ 20) indicates the prevalence of
566 anoxic conditions at the bottom in this period due to the control by sulfide

567 concentrations (Huerta-Diaz and Morse, 1992; Chaillou et al., 2002; Nameroff et al.,
568 2002; Sundby et al., 2004, Tribovillard et al., 2004). Our low U/Mo ratio (~0.3, Fig. 9)
569 corroborates this assumption, as similar to those values reported today at shallower
570 anoxic zones off Perú interrupted by seasonal oxygenation (McManus et al., 2006;
571 Sholz et al., 2011, Salvattecí et al., 2016; Vergara et al., 2016). This is similar to our
572 shelf, notwithstanding the prevalence of very reduced conditions within the sediments.

573 The enhanced reduced conditions, probably sulfidic, before cal BP 6600, favor the
574 accumulation of Mo and Cd over that of U, occurring in anoxic environments where
575 the chemocline is close to the water–sediment interface or above it, allowing the
576 formation of authigenic Mo that exceed the U uptake within the sediments (Algeo and
577 Tribovillard, 2009 and references therein). Re is enriched in less reduced conditions
578 than Mo, resulting in the lowest Re/Mo in this period (Fig. 9). This is congruent with
579 the environmental conditions at the bottom in zones of high productivity and intense
580 upwelling, where sulfidic conditions are developed owing to oxygen consumption in
581 the shallower zones and linked to the OMZ, as occur at northern Chilean regions,
582 where the main productivity is developed over the narrow shelf. Thus, the high
583 productivity before cal BP 6600 could result from a more intense upwelling that
584 generated permanent reduced conditions that became very anoxic at the bottom in this
585 period. Even so, the low oxygen conditions prevailed in the subsequent periods but
586 were less intense than before.

587 After cal BP 6400 until 4500 we obtained little information owing to a gap in the
588 sedimentary record, which made it difficult to visualize changes in the oxygenation
589 and productivity proxies in this interval. However, in the next period (cal BP 4500–
590 1800), we observe that the opal accumulation was lower than in the previous recorded
591 period, $12 \pm 4 \text{ g m}^{-2} \text{ y}^{-1}$ (range: $6\text{--}20 \text{ g m}^{-2} \text{ y}^{-1}$, peaking at cal BP 3400–4000; Fig. 9),
592 which is partially consistent with nutrient-type element distributions and element
593 enrichment (Fig. 8a, Fig. 9). Fe clearly shows higher values at approximately cal BP
594 3500 (Fig. 8a), which helped to boost primary productivity at this time, with a small
595 increase in diatom, measured as valves per gram and abundance (%) (Fig. 6). Other
596 elements showed less prominent accumulations (Ni, Cd, Ba, Ca, and P), pointing to a
597 lower organic matter deposition into the sediments during this period (Fig. 8a). Thus, a
598 decreasing trend in the primary productivity from cal BP 6600 is observed, which is
599 also consistent with observations off south-central Chile (36° S , Concepción shelf)

600 where lower accumulations of nutrient-type elements were also observed at cal BP
601 3600–4000 and cal BP 2600 than at cal BP 6200 (Muñoz et al., 2012).

602 The low oxygen conditions within the sediments were maintained, despite the
603 downward trend in the primary productivity. This could be more related to the
604 manifestation of the OMZ close to the coast than the oxygen consumption during
605 organic matter remineralization, favoring Mo and Re accumulation until cal BP
606 1700–1800 (Fig. 8a). Lower Cd/U ratios (~ 1 ; Fig. 9) were estimated, suggesting higher
607 variations in the primary productivity but with moderate changes in the oxygen
608 conditions at the bottom. High Re/Mo and U/Mo ratios could indicate a shift toward
609 less reduced conditions but still anoxic, since U, Re, and Mo are highly enriched (6,
610 20, and 15, respectively; Fig. 9). U and Re accumulations occur in conditions that
611 exhibit less intense reduction but are not very favorable for Mo accumulation
612 (Morford et al., 2009). This could be caused by a lower C rain rate due to lower
613 productivity, producing low oxygen consumption and a less sulfidic environment
614 along the central-Chilean margin (30–36° S), which is in agreement with the lower
615 biogenic opal flux and diatom abundance after cal BP 6600 (Figs. 6, 9).

616 Slight increasing values of Re/Mo ratios until \sim cal BP 3500 suggest a decreasing trend
617 in the reduced conditions, which became stronger after cal BP 1800. This time was
618 also highlighted in the sedimentary records off Concepcion shelf (36° S, Muñoz et al.,
619 2012) showing maximum enrichment of U and Cr near cal BP 1800, both indicating
620 less reduced conditions toward the present compared with previous periods. After this
621 age, no comparison could be made owing to a discontinuity in the sedimentary records
622 off Concepción. Notwithstanding, the suboxic conditions have prevailed until today at
623 Central Chile, where the oxygenation seems has been stronger off Coquimbo. It could
624 be caused by eddies related to the instabilities of the Peru Undercurrent (Vergara et al.,
625 2016), which seem to start operating more frequently from cal BP 1800 to the present.
626 After this age to cal BP 140, higher productivities were not found, and a second
627 discontinuity (cal BP 1500–240) impeded environmental reconstructions, with the
628 very low estimated sedimentation rate hindering the realization of sufficient time
629 resolution for the proxies in this interval.

630 After cal BP \sim 140 to recent times (CE 2015) (third period mentioned before), the
631 productivity increased substantially, deduced from the rise in opal accumulations

632 toward the present (mean opal value of $29 \pm 17 \text{ g m}^{-2} \text{ y}^{-1}$, range: $10\text{--}69 \text{ g m}^{-2} \text{ y}^{-1}$; Fig.
633 9); however, this corresponded with lower diatom abundances, which were observed
634 from cal BP 1800 to the present (range: $0.5\text{--}4.9 \times 10^6 \text{ valves g}^{-1}$; Fig. 6). This is likely
635 caused by the fact that only a few sections of the core in this interval were analyzed
636 for diatoms, leading to a low resolution for this measurement in the most recent
637 period. Another possibility is that the opal flux was overestimated owing to the fact
638 that the flux calculations were based on recent sedimentation rates, an estimation that
639 tends to be higher than at longer timescales (Sadler et al., 1999). However, the slight
640 increase in the Cd/U ratio, Ba and P enrichment could suggest an increase in the
641 primary productivity and organic fluxes to the bottom in more recent times (Figs. 8,
642 9). In addition, the main trend established before and after the hiatus indicates an
643 increase in the marine productivity, which would not be as high as in the first period
644 (before cal BP 6600). After cal BP 1800, there is an evident change to a less reduced
645 environment toward the present, suggesting a more oxygenated bottom environment
646 concurrent with a reduction in primary productivity, except for the last 140 years,
647 when the productivity has been more variable with a slight increasing trend.

648 Contrary to other metals, there is a conspicuous upward trend for Cu/Al, Fe/Al, and
649 Mn/Al in recent times, which is consistent with the decreasing trend of EFs of Re, U,
650 and Mo (Fig. 8a, 8b, Fig. 9); these estimations would not be influenced by the
651 sedimentation rates but rather the presence of oxygen. Otherwise, the highest
652 enrichment of Cu could suggest the presence of particulate forms and oxide formation
653 (Peacock and Sherman, 2004; Vance et al., 2008; Little et al., 2014) occurring in the
654 presence of an oxygenated environment that results in a high metal enrichment of Cu
655 ($\text{EF}_{\text{Cu}} = 4.6 \pm 0.5$, Fig. 9); however, suboxic conditions have prevailed, indicated by
656 the U/Mo ratios in the range of the reduced sediments, which are less than in the
657 sediments of the Peru shelf (Scholz et al., 2011; Salvattecchi et al., 2016). In addition,
658 the Cu enrichment coincides with the growing trend of industrialization in the area,
659 mainly the mining activity, which has been the main economic source for Coquimbo
660 region since 1890; therefore, the exposition of mineral ores and mine residues to the
661 environment by natural processes as intemperization and wind transportation deserve
662 attention.

663 We suggest that the slightly higher productivity in the last 140 years has occurred in a
664 more oxygenated environment, which seems contradictory. However, similar OMZ

665 weakening has been described off Central Peru from 1875 to 2004, caused by a
666 balance between the local productivity and the subsurface ventilation of the
667 intermediate circulation, operating at (multi)decadal to centennial scale, and hence
668 related to IPO and ENSO (Cardich et al., 2019). Current studies have shown that
669 changes in both the Peru-Chile Undercurrent (PCUC) and mesoscale eddy field
670 contribute to modulate the vertical and offshore extension of the OMZ at intra-
671 seasonal and seasonal time scales off central Chile (e.g. Vergara et al., 2016; Frenger
672 et al., 2018; Pizarro-Koch et al., 2019) and possibly at lower frequencies, modulating
673 the influence of the OMZ over the coastal zones. In addition, ENSO has been
674 identified as an important mechanism of the OMZ ventilation in the Tropical South
675 Eastern Pacific through horizontal and vertical eddy fluxes; thus, during El Niño, the
676 coastal trapped waves propagate poleward and the water column becomes oxygenated,
677 and contrarily deoxygenated during the La-Niña like conditions (Espinoza-Morriberón
678 et al., 2019 and references therein).

679 Several observations made at central Peruvian and south-central Chilean coasts
680 (12° – 36° S) reveal that the present-day wet/dry variability associated with ENSO has
681 a strong impact on the benthic communities. During El Niño, the large increase in the
682 oxygen levels change the biogeochemical processes at the bottom and its effects can
683 be observed several months after the event (Ulloa et al., 2001; Escribano et al., 2004;
684 Gutiérrez et al., 2006; 2008; Sellanes et al., 2007). Thus, the increased frequency and
685 intensity of El Niño at recent centuries would result in a mean effect, which is
686 observed as a gradual change in metal enrichment over time. This is explained by the
687 episodic oxygenation, which changes the original extent of the accumulation of
688 sensitive redox trace element through their remobilization to soluble forms (Morford
689 and Emerson, 1999; Morford et al., 2009).

690 The strong trend towards increasingly reduced conditions in the northern margin of the
691 SE Pacific (Peru and north of Chile) in the past decades has been explained by a
692 greater impact of local productivity on coastal hypoxia (Cardich et al., 2019; Díaz-
693 Ochoa et al., 2011), something that is not clearly observed in our records. Contrarily, a
694 gradual oxygenation in the north-central Chilean margin was observed, which may
695 rather respond to the deepening of the OMZ. The oxygenation/deoxygenation
696 mechanism can be the result of coastal-trapped waves, originating from the equator
697 and propagating along the coast, at different time scales and intensities. These modify

698 the stability of the regional current system and the pycnocline, and can trigger extra-
699 tropical Rossby waves (Pizarro et al., 2002; Ramos et al., 2006; 2008), contributing to
700 the oxygen variability in coastal zones, with a major impacts on redox-sensitive
701 elements in the surface sediments.

702

703 **5.3. Main climatic implications**

704 According to paleoenvironmental records, the past climate and oceanographic
705 variability have been interpreted mainly based on the past variability in the intensity of
706 the SWW and latitudinal position of the ITCZ (Veit et al., 1996; Hebbeln et al., 2002;
707 Lamy et al., 1999; Maldonado and Villagrán, 2002). The ITCZ movements from the
708 northernmost or southernmost latitudinal position depend on the different phases of
709 ENSO and PDO variability (Yang and Oh, 2020), as the main regulators of the climate
710 at the centennial and decadal scales. This has an impact over relevant oceanographic
711 characteristics, such as sea surface temperature (SST), upwelling, and accordingly,
712 productivity at the SE Pacific. We established marked differences in paleo-productivity
713 proxies and paleo-oxygenation in the last ~8000 years (Figs. 6, 8), indicating that high
714 marine productivity prevailed during our first period (cal BP 8000–6600), according to
715 what was established for central Chile between 10 and 5 ky owing to sustained mean La
716 Niña-like conditions associated with the cold phase of the PDO (positive phase) (De
717 Pol-Holz et al., 2006; Kaiser et al., 2008; Lamy et al., 2010), concomitantly with
718 reduced ENSO variability and a northward ITCZ displacement, which implies more
719 permanent southeast trade winds and, hence, the upwelling of rich-nutrient cold waters
720 at eastern Pacific (Koutavas and Lynch-Stieglitz, 2004; Koutavas et al., 2006; Koutavas
721 et al., 2014).

722 Our high productivity records associated with low oxygen conditions at the bottom,
723 both reaching a maximum level at cal BP 6600, correspond to the highest productive
724 period and the most reductive environment at the bottoms over the past 8000 y. The
725 continental climate during this period has been described as being drier, with the
726 predominance of La Niña-like conditions according to the northerly position of the
727 ITCZ, which promote strong upwelling due to persistent southeast trades. This climatic
728 condition has been described for the tropical Pacific and SE Pacific (Lamy et al., 2001;
729 Carré et al., 2012; Koutavas et al. 2014; Salvatecci et al., 2019), indicating that La Niña-
730 like conditions, developed at the mid-Holocene, resulted from an intensification of the

Comentario [A10]: It should say ,
Koutavas and Joanides, 2012

Comentario [A11]: It should say: 2006

Comentario [A12]: It should say
Salvattecci

731 SPSA and the Walker circulation. These environmental conditions are in agreement
732 with the observations of our pollen records and productivity proxies (PMI, Fig. 9),
733 establishing favorable conditions for upwelling and development of primary
734 productivity along the South-East Pacific margin.

735 For central Chile, the aridity conditions were limited until cal BP 5700 (Jenny et al
736 2002, Maldonado and Villagrán, 2006) or cal BP 4200 (Maldonado and Rozas, 2008;
737 Maldonado and Villagrán, 2002, 2006), characterized by reduced rainfall but intense
738 coastal humidity, which have been associated with coastal fogs that frequently occur
739 during the spring owing to a strengthening of the SPSA (Vargas et al., 2006; Garreaud
740 et al 2008; Ortega et al., 2012) and La Niña-like conditions, which explains the main
741 variability of the SPSA (Ancapichún and Garcés-Vargas, 2015). Similarly, for southern
742 Chile (41°S; Lamy et al., 2001), less humid conditions were described for a period
743 between cal BP 7700 and cal BP 4000, being stronger between cal BP 6000 and cal BP
744 5300, by a poleward position of the Southern Westerlies. All of this points to drier
745 conditions during the mid-Holocene, which was closely related to SPSA intensification
746 and the southern position of the Southern Westerlies.

747 Consistent with this, a reduced ENSO variance during the early and mid-Holocene has
748 been suggested (Rein et al., 2005), indicating a less frequent or less intense warm
749 anomaly related to a Central Pacific (CP)-mode ENSO, which produce a moderate El
750 Niño events at the CP and strong La Niña off Peru (Carré et al., 2014, Mollier-Vogel et
751 al., 2019). This was favorable for upwelling and primary productivity development
752 along the Chilean and Peruvian margin. In addition, Braconnot et al. (2012) indicated
753 that this lower ENSO was linked to fresh water melting that counteracted the insolation
754 regime, pointing a more limited cold-dry period between 6700–7500 years ago, which
755 matches our records of maximum productivity (Figs. 6, 9) concomitantly with the
756 lowest bottom oxygen conditions and indicates a greater influence of the OMZ over the
757 shelf at the central-Chilean margin.

758 After the maximum productivity recorded, a decreasing trend occurred under warm and
759 humid climatic conditions, which would be because of an enhancement in regional
760 precipitation in the northern margin of SWW (Jenny et al., 2003; Maldonado and
761 Villagrán, 2006), consistent with the southern movement of the ITCZ, leading to wetter
762 climatic conditions in the southern tropics regions (Koutavas and Lynch-Stieglitz,

763 2004). A gradual rise in K/Ca, Fe, Al, and Pb distributions was observed in our cores
764 (Figs. 5, 9), usually considered to be an indicator of continental input by fluvial or aerial
765 transport (Calvert and Pedersen, 2007; Kaiser et al., 2008; Govin et al., 2012; Ohnemus
766 and Lam, 2015; Saito et al., 1992; Xu et al., 2015). This indicated that the precipitation
767 has been increasing through the mid- and late Holocene, except for a period of reduced
768 (or weak) ENSO activity reported between cal BP 6000 and 4000 (Koutavas and
769 Joanides, 2012; Carré et al., 2014). It is also consistent with the pollen records of central
770 Chile, which suggest an arid phase from cal BP 6200 until cal BP 4200 (Maldonado and
771 Villagrán, 2006). The lack of records between these ages in our cores (hiatus) prevented
772 the search for evidence to account for this period; consequently, no sharply contrasting
773 dry/humid periods were identified after cal BP 6600. Mostly, a gradual increase in
774 humidity and a weakening in paleo-productivity proxies after cal BP 4500 (Figs. 8, 9)
775 were observed, which would be consistent with the beginning of higher ENSO
776 variability for central-Chile after cal BP 5700 (Jenny et al., 2002, Maldonado and
777 Villagrán, 2002, 2006).

778 In general, the weakening of the SPSA results in a equatorward position of the Southern
779 Westerlies increasing the humidity conditions in Central Chile (Lamy et al., 2001), and
780 the ENSO variability increased from cal BP 5700, and stronger El Niño events would
781 begin after cal BP 4000–4500; concomitant with the high variability of latitudinal
782 displacements of the ITCZ related to the seasonality of insolation described for the
783 region at the mid- and late Holocene (Haug et al., 2001; Toth et al., 2012; Carré et al.,
784 2014). This is consistent with the occurrence of alluvial episodes in the area caused by
785 more frequent or heavier rainfall events over time, related to intensified Westerlies and
786 increased El Niño events observed from Peru to south of Chile (Lamy et al., 2001;
787 Jenny et al., 2002; 2003; Rein et al., 2005; Sandweiss et al., 2007; Ortega et al., 2012;
788 Ortega et al., 2019). A consequence is greater continental inputs, as suggested by our
789 sedimentary records in agreement with the pollen moisture index that indicated more
790 humid conditions through the mid-Holocene to the present. This was concomitant with
791 greater oxygenation at the bottom and reduced primary productivity. Nonetheless,
792 between cal BP 4500 and 3000, a slight increase in diatom abundance and opal
793 concentrations was observed, along with a slight accumulation in nutrient elements (Ni,
794 Cd, Fe, and Ca concentrations; Fig. 8). Small increases in the organic carbon flux and
795 Cd/U ratios (Fig. 5, 9) suggest that the increase in primary productivity could be

796 boosted by continental nutrients (Dezileau et al., 2004; Kaiser et al., 2008). This period
797 has been documented for the tropical east Pacific as a peak of La Niña activity (cal BP
798 3000–4000; Toth et al., 2012). This would also explain the increase in the productivity
799 proxies.

800 Despite the dominance of warm events described from the mid- to late Holocene, they
801 were not strong enough to change the suboxic conditions at the bottom in the north-
802 central Chilean margin, which varied little until cal BP 1800 (Figs. 8, 9; see U, Mo, and
803 Re). Actually, the periodicity of El Niño was similar between cal BP 5000 and cal BP
804 3000 and lower than modern times (Sandweiss et al., 2007), supporting the observation
805 of relatively low variability of the oxygen proxies in the sediments dependent on the
806 OMZ influence over the shelf. This implies that the upper limit location of the OMZ did
807 not drastically change during most of the mid- and late Holocene. Contrary to our
808 observations, the sediments at the Peruvian shelf were less reduced in the late-mid
809 Holocene than at present, which was due to a deepening in the OMZ by the increased
810 advection of waters enriched in oxygen from the Equatorial Undercurrent and the
811 shifting of the OMZ center toward the Chilean margin, leaving lower $\delta^{15}\text{N}$ values in
812 sedimentary records off Peru (Mollier-Vogel et al., 2019). Therefore, the enhanced
813 oxygenation of Peru and OMZ deepening translated into a decrease in the oxygen
814 conditions off north-central Chile. This period is followed by an increased El Niño
815 frequency that has been consistent with the intensification and frequency of flooding
816 events recorded in Peru and central Chile in the last ~2000 years (Rein et al., 2005;
817 Sandweiss et al., 2007; Jenny et al., 2002; Toth et al., 2012), which is concomitant with
818 the drastic oxygenation at the bottom observed in our records after cal BP 1800. In this
819 regard, the oxygen variation at the bottom would be related to a less intense effect of the
820 OMZs over the shelf at the central Chilean margin during the warm El Niño-like phases,
821 owing to a deepening of the oxycline (and vice versa during La Niña). These tend to be
822 associated with low productivity and, in turn, a reduction in the organic fluxes and
823 oxygen consumption during organic matter diagenesis.

824 After cal BP 1800, few records were obtained until cal BP 140, when we observed the
825 restoration of more reduced conditions, although lower than during previous periods.
826 This corresponds to the time of Peruvian upwelling shift due to the northward
827 displacement of the ITCZ to the modern position and the enhancement of the Walker

828 circulation (Gutiérrez et al., 2009), which establishes an intensification of the upwelling
829 in the eastern Pacific; consequently, an increase in the primary productivity, producing
830 high demand for oxygen during organic matter remineralization, as observed today,
831 which leads to stronger oxygen consumption in the northern part of the eastern margin.
832 Notwithstanding, the reduced conditions off Coquimbo in recent decades, are not
833 comparable to the environmental conditions of Peruvian margin, where stronger
834 deoxygenation has been developed at the bottom.

835

836 **6. Conclusions**

837 Our results suggest that the geochemistry and sedimentary properties of the coastal
838 shelf environments in north-central Chile have changed considerably during the
839 Holocene period, suggesting two relevant changes in the redox conditions and
840 productivity, which point to a more reducing environment and higher productivity
841 around cal BP 6600. Afterwards, a less reducing environment along with decreasing
842 trends in primary productivity and increased humid conditions occurs with time. The
843 oxygenation of the surface limit of the OMZ has been proposed as the main
844 mechanism that controls the reduced conditions over the shelf and slope sediments
845 during the mid-Holocene, which mainly affected the Peruvian margin closed to the
846 OMZ edge. This led to contrasting conditions in the central-Chilean margin where the
847 most reduced conditions were observed, which was maintained with low variability
848 until cal BP 1800. After this age, the OMZ expression over the shelf was weak,
849 returning to more reduced conditions in recent times (two last centuries), similar to the
850 Peruvian margin but weaker at north-central Chile.

851 The northward shifts of the SWW belt, in addition to an increased frequency in El Niño
852 events, have been proposed as the main drivers for climatic conditions during this
853 period. These elements have introduced high variability in the primary productivity
854 during this time interval. This also impacted the accumulation of organic matter due to
855 an intensification of its remineralization, showing a decreasing trend in the buildup of
856 nutrient-type elements and organic carbon burial rates toward the present. Otherwise,
857 decreasing oxygen content at the bottom is highly influenced during El Niño events,
858 something that seems to have been operating at higher frequencies after cal BP 1800
859 and, especially after cal BP 140, when the most extreme events become more frequent.
860 Thus, the El Niño phenomenon and ITCZ latitudinal displacement have greatly
861 contributed to the climatic and oceanographic features in the eastern Pacific, linked to

862 the positive or negative phases of the PDO, which all has a relevant effect on the OMZ
863 position in the Chilean margin. Otherwise, oxygenation/deoxygenation changes can
864 result from coastal-trapped waves that can operate at different time scale and intensities,
865 and have strong effect on the stability of the regional current system and the pycnocline
866 position in the coastal zones.

867 Finally, these changes highlight the sensitivity of these environments to climate
868 variability at different timescales, which is consistent with the description of past
869 regional climatic trends. Based on the dramatic changes observed in the past centuries,
870 future changes are expected in the context of global warming at unprecedented rates.

871

872 7. References

873 Abrantes, F.: Diatom assemblages as upwelling indicators in surface sediments off
874 Portugal, *Mar. Geol.*, 85(1), 15–39, doi:10.1016/0025-3227(88)90082-5, 1988.

875

876 Ancapichún, S. and Garcés-Vargas, J.: Variability of the Southeast Pacific Subtropical
877 Anticyclone and its impact on sea surface temperature off north-central Chile

878 Variabilidad del Anticiclón Subtropical del Pacífico Sudeste y su impacto sobre

879 la temperatura superficial del mar frente a la costa centro-norte de Chile, *Cienc. Mar.*,
880 41(1), 1–20, doi:10.7773/cm.v41i1.2338, 2015.

881

882 Appleby, P. G. and Oldfield, F.: The calculation of lead-210 dates assuming a constant
883 rate of supply of unsupported ²¹⁰Pb to the sediment, *Catena*, 5(1), 1–8,

884 doi:10.1016/S0341-8162(78)80002-2, 1978.

885

886 Bevington, P. and Robinson, K. (Eds.): Error analysis. In: *Data Reduction and Error
887 Analysis for the Physical Sciences*, WCB/McGraw-Hill, USA, 38–52, 1992

888

889 Blanco, J.L., Carr, M-E., Thomas, A.C. and Strub, T.: Hydrographic conditions off
890 northern Chile during the 1996–1998 La Niña and El Niño events, *J. Geophys. Res.*,

891 107, C3, 3017, 10.1029/2001JC001002, 2002.

892

893 Blott, S. J. and Pye, K.: Gradistat: A Grain Size Distribution and Statistics Package for
894 the Analysis of Unconsolidated Sediments, *Earth Surf. Process. Landforms*, 26, 1237–

895 1248, doi:10.1002/esp.261, 2001.

Comentario [A13]: Add missing reference:
Algeo, T.J. and Tribovillard, N.: Environmental analysis of paleoceanographic systems based on molybdenum-uranium covariation, *Chem. Geol.*, 268, 211–225, 2009.

Comentario [A14]: Add missing reference:
Blaauw, M. and Christen, J.: Flexible paleoclimate age-depth models using an autoregressive gamma process. *Bayesian Anal.*, 6, 457–474, 2011.

896
897 Böning, P., Brumsack, H-J., Schnetger, B. and Grunwald, M.: Trace element
898 signatures of Chilean upwelling sediments at 36°S, *Mar. Geol.*, 259, 112–
899 121, [2009](#).
900
901 Böning, P., Shaw, T., Pahnke, K., Brumsack H-J.: Nickel as indicator of fresh organic
902 matter in upwelling sediments. *Geochim. Cosmochim. Ac.*, 162, 99–108, 2015.
903 Braconnot, P., Luan, Y., Brewer, S. and Zheng, W.: Impact of Earth's orbit and
904 freshwater fluxes on Holocene climate mean seasonal cycle and ENSO characteristics,
905 *Clim. Dyn.*, 38, 1081–1092, doi: 10.1007/s00382-011-1029-x, [2012](#).
906
907 Cardich, J., Sifeddine, A., Salvattecchi, R., Romero, D., Briceño-Zuluaga, F., Graco, M.,
908 Anculle, T., Almeida, C. and Gutiérrez, D.: Multidecadal Changes in Marine
909 Subsurface Oxygenation Off Central Peru During the Last ca. 170 Years, *Front. Mar.*
910 *Sci.*, 6(270), 1–16, doi: 10.3389/fmars.2019.00270, 2019.
911
912 Calvert, S. E. and Pedersen, T. F.: Chapter Fourteen Elemental Proxies for
913 Palaeoclimatic and Palaeoceanographic Variability in Marine Sediments: Interpretation
914 and Application, *Dev. Mar. Geol.*, 1(7), 567–644, doi:10.1016/S1572-5480(07)01019-6,
915 [2007](#).
916
917 Carré, M., Sachs, J.P., Purca, S., Schauer, A.J. and Braconnot, P., Falcón, R.A., Julien,
918 M., Lavallée, D.: Holocene history of ENSO variance and asymmetry in the eastern
919 tropical Pacific, *Science* 345, 1045–1048. DOI: 10.1126/science.1255768. 2014.
920
921 Carré, M., Jackson, D., Maldonado, A., Chase, B.M. and Sachs, J.P.: Variability of 14C
922 reservoir age and air–sea flux of CO₂ in the Peru–Chile upwelling region during the
923 past 12,000 years, *Quat. Res.*, 85, 87–93, 2016.
924
925 Chaillou, G., Anschutz, P., Lavaux, G., Schäfer, J. and Blanc, G.: The distribution of
926 Mo, U, and Cd in relation to major redox species in muddy sediments of the Bay of
927 Biscay, *Mar. Chem.*, 80(1), 41–59, doi:10.1016/S0304-4203(02)00097-X, 2002.
928

Comentario [A15]: Add missing reference:
Böning, P., Shaw, T., Pahnke, K., Brumsack H-J.: Nickel as indicator of fresh organic matter in upwelling sediments. *Geochim. Cosmochim. Ac.*, 162, 99–108, 2015.

Comentario [A16]: Add missing reference:
Braconnot, P., Luan, Y., Brewer, S. and Zheng, W.: Impact of Earth's orbit and freshwater fluxes on Holocene climate mean seasonal cycle and ENSO characteristics. *Clim. Dyn.*, 38, 1081–1092, doi: 10.1007/s00382-011-1029-x, 2012.

Comentario [A17]: Add missing reference:
Carré, M., Azzoug, M., Bentaleb, I., Chase, B.M., Fontugne, M., Jackson, D., Ledru, M-P., Maldonado, A., Sachs, J., Schauer, A.: Mid-Holocene mean climate in the south eastern Pacific and its influence on South America, *Quat. Int.*, 253, 55–66, 2012.

929 Colodner, D., Sachs, J., Ravizza, G., Turekian, K. K. and Boyle, E.: The geochemical
930 cycle of Re: a reconnaissance, *Earth Planet. Sci. Lett.*, 117, 205–221, doi:10.1016/0012-
931 821X(93)90127-U, 1993.

932

933 Croquette, M., Eldin, G., Grados, C. and Tamayo, M.: On differences in satellite winds
934 product and their effects in estimating coastal upwelling processes in the South-east
935 Pacific, *Geophys. Res. Lett.*, 34 L11 608, doi: 10.1029/2006GL027538. 2007.

936

937 Crusius, J., Calvert, S., Pedersen, T. and Sage, D.: Rhenium and molybdenum
938 enrichments in sediments as indicators of oxic, suboxic and sulfidic conditions of
939 deposition, *Earth Planet. Sci. Lett.*, 145(1–4), 65–78, doi:10.1016/S0012-
940 821X(96)00204-X, 1996.

941

942 Daneri, G., Dellarossa, V., Quiñones, R., Jacob, B., Montero, P. and Ulloa, O.: Primary
943 production and community respiration in the Humboldt Current System off Chile and
944 associated oceanic areas, *Mar. Ecol. Prog. Ser.*, 197, 41–49, doi:10.3354/meps197041,
945 2000.

946

947 De Pol-Holz, R., Ulloa, O., Dezileau, L., Kiser, J., Lamy, F., Hebbeln, D.: Melting of
948 the Patagonian Ice Sheet and deglacial perturbations of the nitrogen cycle in the eastern
949 South Pacific, *Geophys. Res. Lett.*, 33, L04704, doi: 10.1029/2005GL024477, 2006.

950

951 De Pol-Holz, R., Ulloa, O., Lamy, F., Dezileau, L., Sabatier, P., and Hebbeln, D.: Late
952 Quaternary variability of sedimentary nitrogen isotopes in the eastern South Pacific
953 Ocean, *Paleoceanography*, 22, PA2207, doi: 10.1029/2006 PA001308, 2007.

954

955 De Pol-Holz, R., Robinson, R.S., Hebbeln, D., Sigman, D.M., Ulloa, O.; Controls on
956 sedimentary nitrogen isotopes along the Chile margin, *Deep Sea Res. Part II: Topical
957 Studies in Oceanography*, 56, 1042–1054, <https://doi.org/10.1016/j.dsr2.2008.09.014>,
958 2009.

959

960 Dezileau, L., Ulloa, O., Hebbeln, D., Lamy, F., Reyss, J. L. and Fontugne, M.: Iron
961 control of past productivity in the coastal upwelling system off the Atacama Desert,
962 Chile, *Paleoceanography*, 19(3), doi:10.1029/2004PA001006, 2004.

Comentario [A18]: Delete uncited references

Comentario [A19]: Add missing reference:
Díaz-Ochoa, J.A., Pantoja, S., De Lange, G.J., Lange, C.B., Sánchez, G.E., Acuña, V.R., Muñoz, P., Vargas, G.: Oxygen variability in Mejillones Bay, off northern Chile, during the last two centuries, *Biogeosciences*, 8, 137–146, 2011.

963
964 Dymond, J., Suess, E. and Lyle, M.: Barium in deep-sea sediment: A geochemical
965 proxy for paleoproductivity, *Paleoceanography*, 7(2), 163–181, 1992.
966
967 Escribano, R., Daneri, G., Farías, L., Gallardo, V. A., González, H. E., Gutiérrez, D.,
968 Lange, C. B., Morales, C. E., Pizarro, O., Ulloa, O. and Braun, M.: Biological and
969 chemical consequences of the 1997-1998 El Niño in the Chilean coastal upwelling
970 system: A synthesis, *Deep. Res. Part II Top. Stud. Oceanogr.*, 51(20–21), 2389–2411,
971 doi:10.1016/j.dsr2.2004.08.011, 2004.
972
973 Espinoza-Morriberón, D., Echevin, V., Colas, F., Tam, J., Gutierrez, D., Graco, M.,
974 Ledesma, J. and Quispe-Ccalluari, C.: Oxygen variability during ENSO in the Tropical
975 South Eastern Pacific, *Front. Mar. Sci.*, 5(526), 1–20, doi: 10.3389/fmars.2018.00526,
976 2019.
977
978 Faegri, K. and Iversen, J.: Textbook of pollen analysis, IV. The Blackburn Press, New
979 Jersey, 328 pp., 1989.
980
981 Figueroa, D. and Moffat, D.: On the influence of topography in the induction of coastal
982 upwelling along the Chilean coast, *Geophys. Res. Lett.* 27, 3905-3908, 2000.
983
984 Flynn, W. W.: The determination of low levels of polonium-210 in environmental
985 materials, *Anal. Chim. Acta*, 43, 221–227, 1968.
986
987 Frenger, I., Bianchi, D., Sührenberg, C., Oschlies, A., Dunne, J., Deutsch, C., Galbralth,
988 E. and Schütte, F.: Biogeochemical role of subsurface coherent eddies in the ocean:
989 Tracer cannonballs, hypoxic storms, and microbial stewpots?, *Global Biogeochem. Cy.*,
990 32, 226–249. <https://doi.org/10.1002/2017GB005743>, 2018.
991
992 Gallardo, M.A., González, A., Ramos, M., Mujica, A., Muñoz, P., Sellanes, J. and
993 Yannicelli, B.: Reproductive patterns in demersal crustaceans from the upper boundary
994 of the OMZ off north-central Chile, *Cont. Shelf. Res.* 141, 26–37, 2017.
995

996 Ganeshram, R.S., Pedersen, T. F., Calvert, S.G., McNeill, G. and Fontugne, M.:
997 Glacial-interglacial variability in denitrification in the world's oceans: Causes and
998 consequences, *Paleoceanography*, 15(4), 361– 376, 2000.
999
1000 Garreaud, R., Barichivich, J., Christie, D. and Maldonado, A.: Interannual variability of
1001 the coastal fog at Fray Jorge relict forest in semiarid Chile, *Journal of Geophysical*
1002 *Research*. Vol 113. G04011, doi:10.1029/2008JG000709. 2008.
1003
1004 Garreaud, R., Vuille. M., Compagnucci, R. and Marengo, J.: Present-day South
1005 American climate, *Palaeogeogr. Palaeoclimatol.*, 281, 180-195,
1006 doi:10.1016/j.palaeo.2007.10.032, 2009
1007
1008 Gergis, J.L. and Fowler, A.M.: A history of ENSO events since A.D. 1525: implications
1009 for future climate change, *Clim. Change*, 92,343–387, doi: 10.1007/s10584-008-9476-z,
1010 2009.
1011
1012 Govin, A., Holzwarth, U., Heslop, D., Ford Keeling, L., Zabel, M., Mulitza, S., Collins,
1013 J. A. and Chiessi, C. M.: Distribution of major elements in Atlantic surface sediments
1014 (36°N-49°S): Imprint of terrigenous input and continental weathering, *Geochemistry,*
1015 *Geophys. Geosystems*, 13(1), 1–23, doi:10.1029/2011GC003785, 2012.
1016
1017 Grimm, E.: CONISS: a fortran 77 program for stratigraphically constrained cluster
1018 analysis by the method of incremental sum of squares, *Comput. and Geosci.* 13–35,
1019 1987.
1020
1021 Gutiérrez, D., Sifedine, A., Reyss, J.L., Vargas, G., Velazco, F., Salvatelli, R., Ferreira,
1022 V., Ortlieb, L., Field, D., Baumgartner, T., Boussafir, M., Boucher, H., Valdés, J.,
1023 Marinovic, L., Soler, P. and Tapia, P: Anoxic sediments off Central Peru record
1024 interannual to multidecadal changes of climate and upwelling ecosystem during the last
1025 two centuries, *Adv. Geosci.* 6, 119–125, 2006.
1026
1027 Gutiérrez, D., Enríquez, E., Purca, S., Quipuzcoa, L., Marquina, R., Flores, G. and
1028 Graco, M.: Oxygenation episodes on the continental shelf of central Peru: Remote
1029 forcing and benthic ecosystem response, *Prog. Oceanogr.*, 79, 177–189, 2008.

1030
1031 Gutiérrez, D., Sifedine, A., Field, D.B., Ortlieb, L., Vargas, G., Chávez, F.P., Velazco,
1032 F., Ferreira, V., Tapia, P., Salvattecí, R., Boucher, H., Morales, M.C., Valdés, J., Reys,
1033 J-L., Campusano, A., Boussafir, M., Mandeng-Yogo, M., García, M., and Baumgartner,
1034 T.: Rapid reorganization in ocean biogeochemistry off Peru towards the end of the Little
1035 Ice Age, *Biogeosciences*, 6, 835–848, 2009.
1036
1037 Hansen, H. P. and Koroleff, F.: Determination of nutrients. In *Methods of Seawater*
1038 *Analysis*. Grasshoff, K., Kremling, K. and Ehrhardt, M. (Eds.), Wiley-VCH Verlag
1039 GmbH, Weinheim, Germany, 159–228, 1999.
1040
1041 Haug, G.H., Hughen, K.A., Sigman, D.M., Peterson, L.C. and Röhl, U.: Southward
1042 Migration of the Intertropical Convergence Zone through the Holocene, *Sci.* 293, 1304–
1043 1307, 2001.
1044
1045 Hebbeln, D., Marchant, M., Freudenthal, T. and Wefer, G.: Surface distribution along
1046 the Chilean continental slope related to upwelling and productivity, *Mar.*
1047 *Geol.*, 164, 119–137, 2000.
1048
1049 Hebbeln, D., Marchant, M. and Wefer, G.: Paleoproductivity in the southern Peru ^
1050 Chile Current through the last 33 000 yr, *Mar. Geol.*, 186, 2002.
1051
1052 Helly, J. and Levin, L.: Global distribution of naturally occurring marine hypoxia on
1053 continental margin, *Deep-Sea Res. Pt. I*, 51, 1159–1168, 2004.
1054
1055 Heusser, C. J. and Moar, N. T.: Pollen and spores of Chile: Modern types of the
1056 pteridophyta, gymnospermae, and angiospermae, *New Zeal. J. Bot.*, 11(2), 389–391,
1057 doi:10.1080/0028825X.1973.10430287, 1973.
1058
1059 Jenny, B., Valero-Garcés, B.L., Urrutia, R., Kelts, K., Veit, H., Appleby, P.G., Geyh,
1060 M.: Moisture changes and fluctuations of the Westerlies in Mediterranean
1061 Central Chile during the last 2000 years: The Laguna Aculeo record (33°50'S, *Quat.*
1062 *Int.* 87, 3–18, 2002.
1063

Comentario [A20]: Add missing reference:
Huerta-Díaz, M. A. and Morse, J. W.: Pyritization of trace metals in anoxic marine sediments, *Geochim. Cosmochim. Acta*, 56(7), 2681–2702, doi:10.1016/0016-7037(92)90353-K, 1992.

1064 Jenny, B., Wilhelm, D. and Valero-Garcés, B.L.: The Southern Westerlies in Central
1065 Chile: Holocene precipitation estimates based on a water balance model for Laguna
1066 Aculeo (33°50'S), *Clim. Dynam.*, 20, 269–280, DOI 10.1007/s00382-002-0267-3,
1067 2003.
1068

1069 Kaiser, J., Schefuß, E., Lamy, F., Mohtadi, M. and Hebbeln, D.: Glacial to Holocene
1070 changes in sea surface temperature and coastal vegetation in north central Chile: high
1071 versus low latitude forcing, *Quat. Sci. Rev.*, 27, 2064–2075, 2008.
1072

1073 Koutavas, A. and Joanides, S.: El Niño–Southern Oscillation extrema in the Holocene
1074 and Last Glacial Maximum, *Paleoceanography*, 27, PA4208,
1075 doi:10.1029/2012PA002378, 2012.
1076

1077 Koutavas, A., de Menocal, P.B., Olive, G.C. and Lynch-Stieglitz, J.: Mid-Holocene El
1078 Niño–Southern Oscillation (ENSO) attenuation revealed by individual foraminifera in
1079 eastern tropical Pacific sediments, 34(12), 993–996, doi: 10.1130/G22810A, 2006.
1080

1081 Koutavas, A., and Lynch-Stieglitz, J.: Variability of the marine ITCZ over the
1082 Eastern Pacific during the past 30,000 years. Regional Perspective and Global Context,
1083 in: *The Hadley Circulation*, Diaz, H.F., and Bradley, R.S., Eds. Chapter 12, *Advances in*
1084 *Global Change Research book series (Aglo, volume 21)*, 347–369, 2004.
1085

1086 Lamy F., Hebbeln, D. and Wefer, G.: High-Resolution Marine Record of Climatic
1087 Change in Mid-latitude Chile during the Last 28,000 Years Based on Terrigenous
1088 Sediment Parameters, *Quat. Res.*, 51, 83–93, 1999.
1089

1090 Lamy F., Hebbeln, D., Röhl, U. and Wefer, G.: Holocene rainfall variability in southern
1091 Chile: a marine record of latitudinal shifts of the Southern Westerlies, *Earth Planet Sc.*
1092 *Lett.*, 185, 369–382, 2001.
1093

1094 Lamy, F., Kilian, R., Arz, H.W., Francois J-P., Kaiser, J., Prange, M. and Steinke, T.:
1095 Holocene changes in the position and intensity of the southern westerly wind belt, *Nat.*
1096 *Geosci.*, 3, 695–699, 2010.
1097

1098 Little, S. H., Vance, D., Walker-Brown, C. and Landing, W. M.: The oceanic mass
1099 balance of copper and zinc isotopes, investigated by analysis of their inputs, and outputs
1100 to ferromanganese oxide sediments, *Geochim. Cosmochim. Ac.*, 125, 673–693,
1101 doi:10.1016/j.gca.2013.07.046, 2014.
1102

1103 Maldonado, A. and Rozas, E.: Clima y Paleoambientes durante el Cuaternario Tardío en
1104 la Región de Atacama, in *Libro Rojo de la Flora Nativa y de los Sitios Prioritarios para*
1105 *su Conservación: Región de Atacama*, pp. 293–304., 2008.
1106

1107 Maldonado, A. and Villagrán, C.: Paleoenvironmental changes in the semiarid coast of
1108 Chile (~32°S) during the last 6200 cal years inferred from a swamp-forest pollen
1109 record, *Quat. Res.*, 58, 130–138, 2002.
1110

1111 Maldonado, A. and Villagrán, C.: Climate variability over the last 9900 cal yr BP from
1112 a swamp forest pollen record along the semiarid coast of Chile, *Quat. Res.*, 66(2), 246–
1113 258, doi:10.1016/j.yqres.2006.04.003, 2006.
1114

1115 Mazzullo, J., Leschak, P. and Prusak, D.: Sources and distribution of late Quaternary
1116 silt in the surficial sediment of the northeastern continental shelf of the United States,
1117 *Mar. Geol.*, 78:241–254, 1988.
1118

1119 McManus, J., Berelson, W. M., Severmann, S., Poulson, R. L., Hammond, D. E.,
1120 Klinkhammer, G. P., and Holm, C.: Molybdenum and uranium geochemistry in
1121 continental margin sediments: Paleoproxy potential, *Geochim. Cosmochim. Ac.*, 70,
1122 4643–4662, 2006.
1123

1124 Merino-Campos, V., De Pol-Holz, R., Southon, J., Latorre, C., Collado-Fabbri, S.:
1125 Marine radiocarbon reservoir age along the Chilean continental margin, *Radiocarbon*,
1126 81, 1–16, doi:10.1017/RDC.2018.81, 2018.
1127

1128 Mollier-Vogel, E., Martinez, P., Blanz, T., Robinson, R., Desprat, S., Etourneau, J.,
1129 Charlier, K., Schneider, R. R.: Mid-Holocene deepening of the Southeast Pacific
1130 oxycline, *Global Planet Change*, 172, 365–373, 2019.
1131

Comentario [A21]: It should say:
Mazzullo, J. M. and Graham, A. G.(Eds):
Handbook for Shipboard Sedimentologists,
ODP Tech. Note, 8, 67 pp., 1988.

1132 Montecinos, A., and Aceituno, P.: Seasonality of the ENSO-Related Rainfall Variability
1133 in Central Chile and Associated Circulation Anomalies, *J. Climate.*, 16, 281–296, 2003.
1134
1135 Montecinos, S., Gutiérrez, J. R., López-Cortés, F. and López, D.: Climatic
1136 characteristics of the semi-arid Coquimbo Region in Chile, *J. Arid Environ.*, 126, 7–11,
1137 doi:10.1016/j.jaridenv.2015.09.018, 2016.
1138
1139 Moraga-Opazo, J., Valle-Levinson, A., Ramos, M. and Pizarro-Koch, M.: Upwelling-
1140 Triggered near-geostrophic recirculation in an equatorward facing embayment, *Cont.*
1141 *Shelf Res.*, 31, 1991–1999, 2011.
1142
1143 Morford, J. and Emerson, S.: The geochemistry of redox sensitive trace metals in
1144 sediments, *Geochim. Cosmochim. Ac.*, 63, 11/12, 1735–1750, 1999.
1145
1146 Mortlock, R. A. and Froelich, P. N.: A simple method for the rapid determination of
1147 biogenic opal in pelagic marine sediments, *Deep Sea Res. Part A, Oceanogr. Res. Pap.*,
1148 36(9), 1415–1426, doi:10.1016/0198-0149(89)90092-7, 1989.
1149
1150 Muñoz, P., Dezileau, L., Lange, C., Cárdenas, L., Sellanes, J., Salamanca, M.,
1151 Maldonado A.: Evaluation of sediment trace metal records as paleoproductivity and
1152 paleoxygenation proxies in the upwelling center off Concepción, Chile (36° S). *Prog.*
1153 *Oceanogr.*, Special Issue 92-95, 66-80, 2012.
1154
1155 Nameroff, T., Balistrieri, L. and Murray, W.: Suboxic trace metals geochemistry in the
1156 eastern tropical North Pacific, *Geochim Cosmochim Ac.*, 66(7), 1139–1158, 2002.
1157
1158 Ohnemus, D. C. and Lam, P. J.: Cycling of lithogenic marine particles in the US
1159 GEOTRACES North Atlantic transect, *Deep. Res. Part II Top. Stud. Oceanogr.*, 116,
1160 283–302, doi:10.1016/j.dsr2.2014.11.019, 2015.
1161
1162 Ortega, C., Vargas, G., Rutllant, J.A., Jackson, D. and Méndez, C.: Major hydrological
1163 regime change along the semiarid western coast of South America during the early
1164 Holocene, *Quaternary Res.*, 78, 513-527, 2012.
1165

Comentario [A22]: Add missing reference:
Morford, J.L., Martin, W.R., Francois, R., Carney, C.M.: A model for uranium, rhenium and molybdenum diagenesis in marine sediments based on results from coastal locations, *Geochim. Cosmochim. Ac.*, 73, 2938–2960, 2009.

1166 Ortega, C., Vargas, G., Rojas, M., Rutllant, J.A., Muñoz, P., Lange, C.B., Pantoja, S.,
1167 Dezileau, L. and Ortlieb, L.: Extreme ENSO-driven torrential rainfalls at the southern
1168 edge of the Atacama Desert during the late Holocene and their projection into the 21th
1169 century, *GloPlaCha*, 175, 226 – 237, [https://doi.org/ 10.1016/j.gloplacha.2019.02.011](https://doi.org/10.1016/j.gloplacha.2019.02.011),
1170 2019.
1171
1172 Paytan, A.: Ocean paleoproductivity, *Encyclopedia of Paleoclimatology and Ancient*
1173 *Environments*, Encyclopedia of Earth Science Series, Gornitz, V. (Ed.), Kluwer
1174 Academic Publishers. 2008.
1175
1176 Peacock, C.L. and Sherman, D.M.: Copper(II) sorption onto goethite, hematite and
1177 lepidocrocite: a surface complexation model based on ab initio molecular geometries
1178 and EXAFS spectroscopy, *Geochim. Cosmochim. Ac.*, 68, 2623–2637, 2004.
1179
1180 Pizarro, O., Hormazabal, S., Gonzalez, A. and Yañez, E.: Variabilidad
1181 del viento, nivel del mar y temperatura en la costa norte de Chile, *Invest.*
1182 *Mar.*, 22, 85–101, 1994.
1183
1184 Pizarro, O., Shaffer, G., Dewitte, B. and Ramos, M.: Dynamics of seasonal and
1185 interannual variability of the Peru-Chile Undercurrent, *Geophys. Res. Lett.*, 29(12), 28–
1186 31, doi:10.1029/2002GL014790, 2002.
1187
1188 Pizarro-Koch, M., Pizarro, O., Dewitte, B., Montes, I., Ramos, M., Paulmier, A. and
1189 Garçon, V.: Seasonal variability of the southern tip of the Oxygen Minimum Zone in
1190 the eastern South Pacific (30°-38°S): A modeling study, *J. Geophys. Res. Oceans*, 124,
1191 <https://doi.org/10.1029/2019JC015201>, 2019.
1192
1193 Quintana, J.M. and Aceituno, P.: Changes in the rainfall regime along the extratropical
1194 west coast of South America (Chile): 30-43° S, *Atmosfera*, 25(1), 1 – 22, 2012.
1195
1196 Ramos, M., Pizarro, O., Bravo, L. and Dewitte, B.: Seasonal variability of the permanent
1197 thermocline off northern Chile, *Geophys. Res. Lett.*, 33, L09608,
1198 doi:10.1029/2006GL025882, 2006.
1199

1200 Ramos, M., Dewitte, B., Pizarro, O. and Garric, G.: Vertical propagation of
1201 extratropical Rossby waves during the 1997–1998 El Niño off the west coast of South
1202 America in a medium-resolution OGCM simulation, *J. Geophys. Res.*, 113, C08041,
1203 doi:10.1029/2007JC004681, 2008.
1204
1205 Rahn, D.A. and Garreaud, R.A.: A synoptic climatology of the near-surface wind along
1206 the west coast of South America. *Int. J. Climatol.*, 34(3), 780–792, doi:
1207 10.1002/joc.3724, 2013.
1208
1209 Reimer, P. J., Bard, E., Bayliss, A., Beck, J. W., Blackwell, P. G., Ramsey, C. B., Buck,
1210 C. E., Cheng, H., Edwards, R. L., Friedrich, M., Grootes, P. M., Guilderson, T. P.,
1211 Hafliðason, H., Hajdas, I., Hatté, C., Heaton, T. J., Hoffmann, D. L., Hogg, A. G.,
1212 Hughen, K. A., Kaiser, K. F., Kromer, B., Manning, S. W., Niu, M., Reimer, R. W.,
1213 Richards, D. A., Scott, E. M., Southon, J. R., Staff, R. A., Turney, C. S. M. and van der
1214 Plicht, J.: IntCal13 and Marine13 Radiocarbon Age Calibration Curves 0–50,000 Years
1215 cal BP, *Radiocarbon*, 55(4), 1869–1887, doi:10.2458/azu_js_rc.55.16947, 2013.
1216
1217 Rein, B., Lückge, A., Reinhardt, L., Sirocko, F., Wolf, A. and Dullo, W.-C.: El Niño
1218 variability off Peru during the last 20,000 years, *Paleoceanogr.*, PA4003,
1219 doi:10.1029/2004PA001099, 2005
1220
1221 Rutlland, J. and Fuenzalida, H.: Synoptic aspects of the central Chile Rainfall variability
1222 associated with the southern oscillation, *Int. J. Climatol.*, 11, 63 – 76, 1991.
1223
1224 Rutlland, J. and Montecino, V.: Multiscale upwelling forcing cycles and biological
1225 response off northcentral Chile, *Rev. Chil. Hist. Nat.*, 7, 217–231, 2002
1226
1227 Sabatier, P., Dezileau, L., Blanchemanche, P., Siani, G., Condomines, M., Bentaleb, I.
1228 and Piquès, G.: Holocene variations of radiocarbon reservoir ages in a mediterranean
1229 lagoonal system, *Radiocarbon*, 52(1), 91–102, doi:10.1017/S0033822200045057, 2010.
1230
1231 Sadler, P.M.: The Influence of Hiatuses on Sediment Accumulation Rates, *GeoResearch*
1232 *Forum*, 5, 15–40, 1999.
1233

Comentario [A23]: It should say:
Rutllant

Comentario [A24]: Eliminate uncited
reference

1234 Saito, C., Noriki, S. and Tsunogai, S.: Particulate flux of Ai, a component of land
1235 origin, in the western North Pacific, *Deep-Sea Res.*, 39, 1315–1327, 1992.
1236
1237 [Salvatteci, R., Gutiérrez, D., Field, D., Sifeddine, A., Ortlieb, L., Bouloubassi, I.,
1238 Boussafir, M., Boucher, H. and Cetin, F.: The response of the Peruvian Upwelling
1239 Ecosystem to centennial-scale global change during the last two millennia, *Clim. Past*,
1240 10\(2\), 715–731, doi:10.5194/cp-10-715-2014, 2014.](#)
1241
1242 Salvatteci, R., Gutiérrez, D., Sifeddine, A., Ortlieb, L., Druffel, E., Boussafir, M.,
1243 Schneider, R.: Centennial to millennial-scale changes in oxygenation and productivity
1244 in the Eastern Tropical South Pacific during the last 25,000 years,
1245 *Quat. Sci. Rev.*, 131, 102–117, 2016.
1246
1247 Sandweiss, D.H., Maasch, K.A., Andrus, C. Fred T., Reitz, E.J., Richardson III, J.B.,
1248 Riedinger-Whitmore, M., and Rollins, H.B.: Mid-Holocene climate and culture change
1249 in coastal Peru, Chapter 2, In: *Climate Change and Cultural Dynamics: A Global
1250 Perspective on Mid-Holocene Transitions*, Anderson, D.G., Maasch, K.A., and
1251 Sandweiss, D.H. (Eds.), Elsevier Inc., 25–50, 2007.
1252
1253 Schrader H. J. and Gersonde, R.: Diatoms and silicoflagellates, *Utrecht Micropaleontol.*
1254 *Bull.* 17, 129–176, 1978.
1255
1256 Sellanes, J., Quiroga, E., Neira, C., Gutiérrez, D.: Changes of macrobenthos
1257 composition under different ENSO cycle conditions on the continental shelf off central
1258 Chile, *Cont. Shelf. Res.* 27, 1002–1016, 2007.
1259
1260 Shaffer, G., Pizarro, O. Djurfeldt, L., Salinas, S. and Rutllant, J.: Circulation and low-
1261 frequency variability near the Chilean coast: Remotely forced fluctuations during the
1262 1991– 92 El Niño, *J. Phys. Oceanogr.*, 27, 217– 235, 1997.
1263
1264 Shaffer, G., Hormazabal, S., Pizarro, O. and S. Salinas.: Seasonal and interannual
1265 variability of currents and temperature over the slope of central Chile, *J. Geophys. Res.*,
1266 104, C12, 29,951-29,961, 1999.
1267

Comentario [A25]: Eliminate uncited reference

1268 Scholz, F., Hensen, C., Noffke, A., Rohde, A., Liebetrau, V., Wallmann, K.: Early
1269 diagenesis of redox-sensitive trace metals in the Peru upwelling area – response to
1270 ENSO-related oxygen fluctuations in the water column, *Geochim. Cosmochim. Ac.*, 75,
1271 7257–7276, 2011.
1272
1273 Siebert, C., Nägler, T.F., von Blackenburg, F. and Kramers, J.D.: Molybdenum
1274 isotope records as a potential new proxy for paleoceanography, *Earth Planet. Sci. Lett.*,
1275 6643, 1–13, 2003.
1276
1277 Sigman, D.M., Karsh, K.L. and Casciotti, K.L.: Ocean process tracers: nitrogen isotopes
1278 in the ocean. *Encyclopedia of ocean science*, 2nd edn Elsevier, Amsterdam, 2009.
1279
1280 Sundby, B., Martinez, P. and Gobeil, C.: Comparative geochemistry of cadmium,
1281 rhenium, uranium, and molybdenum in continental margin sediments, *Geochim.*
1282 *Cosmochim. Ac.*, 68, 2485–2493, 2004.
1283
1284 Sweeney, R. E. and Kaplan I. R.: Natural abundances of ¹⁵N as a source indicator of
1285 nearshore marine sedimentary and dissolved nitrogen, *Mar. Chem.*, 9, 81– 94, 1980.
1286
1287 Thiel, M., Macaya, E.C., Acuña, E., Artz, W.F., Bastias, H., Brokordt, K., Camus,
1288 P.A., Castilla, J.C., Castro, L.R., Cortés, M., Dumont, C.P., Escribano, R., Fernandez,
1289 M., Gajardo, J.A., Gaymer, C.F., Gómez, I., González, A.E., González, H.E., Haye, P.,
1290 Illanes, J.E., Iriarte, J.L., Lancellotti, D.A., Luna-Jorquera, G., Luxoro, C., Manriquez,
1291 P.H., Marín, V., Muñoz, P., Navarrete, S.A., Pérez, E., Poulin, E., Sellanes, J.,
1292 Sepúlveda, H.H., Stotz, W., Tala, F., Thomas, A., Vargas, C.A., Vásquez, J.A., Vega,
1293 J.M.: The Humboldt Current system of Northern and Central Chile: Oceanographic
1294 processes, ecological interactions and socioeconomic feedback, *Oceanogr. Mar. Biol.*
1295 *An Annual Review*, 45, 195–344, 2007.
1296
1297 Torres, M. E., Brumsack, H. J., Bohrman, G. and Emeis, K. C.: Barite front in
1298 continental margin sediments: a new look at barium remobilization in the zone of
1299 sulfate reduction and formation of heavy barites in diagenetic fronts, *Chem. Geol.*, 127,
1300 125–139, 1996.
1301

Comentario [A26]: Eliminate uncited reference

1302 Torres, R., and Ampuero, P.: Strong CO₂ outgassing from high nutrient low chlorophyll
1303 coastal waters off central Chile (30°S): The role of dissolved iron, *Estuar. Coast. Shelf*
1304 *S.*, 83, 126–132, doi:10.1016/j.ecss.2009.02.030, 2009.

1305

1306 Toth, L.T., Aronson, R.B., Vollmer, S.V., Hobbs, J.W., Urrego, D.H., Cheng, H.,
1307 Enochs, I.C., Combsch, D.J., van Woesik, R., Macintyre, J.G.: ENSO Drove 2500-
1308 Year Collapse of Eastern Pacific Coral Reefs, *Science* 337, 81– 84, doi:
1309 10.1126/science.1221168, 2012

1310

1311 Tribovillard, N., Algeo, T. J., Lyons, T. and Riboulleau, A.: Trace metals as paleoredox
1312 and paleoproductivity proxies: an update, *Chem. Geol.*, 232, 12–32, 2006.

1313

1314 Ulloa, O., Escribano, R., Hormazabal, S., Quiñones, R.A., Gonzalez, R., Ramos, M.,:
1315 Evolution and biological effects of the 1997-98 El Niño in the upwelling ecosystem off
1316 northern Chile, *Geophys. Res. Lett.*, 28, 1591– 1594, 2001.

1317

1318 Ulloa, O., Canfield, D.E., DeLong, E.F., Letelier, R.L. and Stewart, F.J.: Microbial
1319 oceanography of anoxic oxygen minimum zones, *PNAS*, 109, 15996–16003,
1320 doi/10.1073/pnas.1205009109, 2012.

1321

1322 Vance, D., Archer, C., Bermin, J., Perkins, J., Statham, P. J., Lohan, M. C., Ellwood, M.
1323 J. and Mills, R. A.: The copper isotope geochemistry of rivers and the oceans, *Earth*
1324 *Planet. Sc. Lett.*, 274, 204–213, 2008.

1325

1326 Valle-Levinson, A., Moraga, J., Olivares, J. and Blanco, J. L.: Tidal and residual
1327 circulation in a semi-arid bay: Coquimbo Bay, Chile, *Cont. Shelf. Res.*, 20, 2009–2018,
1328 2000.

1329

1330 Valle-Levinson, A. and Moraga-Opazo, J.: Observations of bipolar residual circulation
1331 in two equatorward-facing semiarid bays, *Cont. Shelf Res.*, 26(2), 179–193,
1332 doi:10.1016/j.csr.2005.10.002, 2006.

1333

1334 Van der Weijden, C.: Pitfalls of normalization of marine geochemical data using a
1335 common divisor, *Mar. Geol.*, 184, 167–187, 2002.

Comentario [A27]: Add missing reference:

Tribovillard, N., Riboulleau, A., Lyons, T., Baudin, F.: Enhanced trapping of molybdenum by sulfurized organic matter of marine origin as recorded by various Mesozoic formations. *Chem. Geol.*, 213, 385–401, 2004.

1336
1337 Vargas, G., Ortlieb, L., Pichon, J. J., Bertaux, J. and Pujos, M.: Sedimentary facies and
1338 high resolution primary production inferences from laminated diatomaceous sediments
1339 off northern Chile (23°S), *Mar. Geol.*, 211(1–2), 79–99,
1340 doi:10.1016/j.margeo.2004.05.032, 2004.
1341
1342 Vargas, G., Rutllant, J., Ortlieb, L.: ENSO tropical–extratropical climate
1343 teleconnections and mechanisms for Holocene debris flows along the hyperarid coast of
1344 western South America (17°–24°S), *Earth Planet. Sci. Lett.*, 249, 467–483, 2006.
1345
1346 Vargas, G., Pantoja, S., Rutllant, J., Lange, C. and Ortlieb, L.: Enhancement of coastal
1347 upwelling and interdecadal ENSO-like variability in the Peru-Chile Current since late
1348 19th century, *Geophys. Res. Lett.*, 34, L13607, 2007.
1349
1350 Vergara, O., Dewitte, B., Montes, I., Garçon, V., Ramos, M., Paulmier, A. and
1351 Pizarro, O.: Seasonal variability of the oxygen minimum zone off Peru in a high-
1352 resolution regional coupled model, *Biogeosciences*, 13, 4389–4410, doi:10.5194/bg-13-
1353 4389-2016, 2016.
1354
1355 Veit, H.: Southern Westerlies during the Holocene deduced from geomorphological and
1356 pedological studies in the Norte Chico, Northern Chile (27–33°S), *Palaeogeogr.,*
1357 *Palaeoclimatol., Palaeoecol.*, 123, 107–119, 1996.
1358
1359 Xu, G., Liu, J., Pei, S., Kong, X., Hu, G. and Gao, M.: Source identification of
1360 aluminum in surface sediments of the Yellow Sea off the Shandong Peninsula, *Acta*
1361 *Oceanol. Sin.*, 34(12), 147–153, doi:10.1007/s13131-015-0766-9, 2015.
1362
1363 Yang, S., and Oh, J-H.: Effects of modes of climate variability on wave power during
1364 boreal summer in the western North Pacific, *Sci. Rep.*, 10:5187, doi:10.1038/s41598-
1365 020-62138-0, 2020.
1366
1367 Zheng, Y., Anderson, R. F., van Geen, A. and Fleisheir, M.Q.: Preservation of non-
1368 lithogenic particulate uranium in marine sediments, *Geochim. Cosmochim. Ac.*, 66,
1369 3085–3092, 2002.

Comentario [A28]: Delete uncited reference

1370
1371
1372
1373
1374
1375
1376
1377
1378
1379
1380
1381
1382
1383
1384
1385
1386
1387
1388
1389
1390
1391
1392
1393
1394
1395
1396
1397
1398
1399
1400
1401
1402
1403

Acknowledgments

We would like to thank the R/V Stella Maris II crew of Universidad Católica del Norte for their help and support during field work. We extend our acknowledgements to the laboratory assistants of the Paleoceanography Lab at Universidad de Concepción for aid in the sample analyses, and to the assistants of the Oceanography Lab of Universidad Católica del Norte for aid in data analysis. We also wish to thank Dr. Olivier Bruguier of CNRS and his lab personnel for their assistance during ICPM analyses. We also express our gratitude to INNOVA 07CN13 IXM-150, FONDECYT 1180413 and FONDECYT 1170408. This manuscript was mainly funded by FONDECYT Project No. 1140851. Partial support from the COPAS Sur-Austral (CONICYT PIA PFB31) and FONDAP-IDEAL centers (No. 15150003) is also acknowledged.

Author contributions: PM prepared the manuscript with contributions from all co-authors. PM, LR and LD developed the proposal and conducted field work. AM, KA and MR assisted in field work in different campaigns. All authors participated in different laboratory work and data analysis, PM, LD and KA conducted metal and radioisotope analyses. MR analyzed physical data and graphs editing. MS helped with alpha counting on prepared samples. CM ran stable isotope and TOC analysis. LR, CL, PC, GS and KL assisted in specimen identifications of foraminifers and diatoms. AM and IJ identified pollen and assisted with the age modeling. GV analyzed physical properties of the sediments and contributed to writing and editing the manuscript.

Competing interests. The authors declare that they have no conflict of interest.

Comentario [A29]: Add missing project code: and AFB170006

1404

1405

1406 **Tables**

1407

1408 Table 1. Radiocarbon dates for BGGC5 and BTGC8 sediment cores collected from
 1409 mixed planktonic foraminifera and monospecific benthic foraminifera (*Bolivina*
 1410 *plicata*), respectively. The ¹⁴C-AMS was performed at NOSAM-WHOI. The lab code
 1411 and conventional ages collected from each core section are indicated. For error
 1412 calculations see <http://www.whoi.edu/nosams/radiocarbon-data-calculations>.

Core identification	Material	Mass (mg)	Lab Code NOSAM	Modern fraction pMC	1σ error	Conventional Age BP	1σ error
Planktonic foraminifera							
BGGC5							
10-11	Mix	1.8	OS-122160	0.8895	0.0027	940	25
18-19	Mix	1.1	OS-122141	0.7217	0.0024	2,620	25
31-32	Mix	2.7	OS-122161	0.6590	0.0021	3,350	25
45-46	Mix	2.0	OS-122162	0.6102	0.0017	3,970	25
55-56	mix	1.6	OS-122138	0.5864	0.0025	4,290	35
66-67	mix	2.8	OS-122304	0.5597	0.0018	4,660	25
76-77	mix	2.6	OS-122163	0.4520	0.0016	6,380	30
96-97	mix	1.1	OS-122139	0.4333	0.0033	6,720	60
115-116	mix	4.7	OS-122164	0.3843	0.0016	7,680	35
Benthic foraminifera							
BTGC8							
5-6	<i>Bolivina plicata</i>	4.2	OS-130657	0.8953	0.0017	890	15
20-21	<i>Bolivina plicata</i>	7.7	OS-123670	0.7337	0.0021	2,490	25
30-31	<i>Bolivina plicata</i>	13.0	OS-123671	0.6771	0.0016	3,130	20
40-41	<i>Bolivina plicata</i>	11.0	OS-123672	0.6507	0.0019	3,450	25
50-51	<i>Bolivina plicata</i>	8.7	OS-123673	0.5877	0.0014	4,270	20
60-61	<i>Bolivina plicata</i>	13.0	OS-123674	0.5560	0.0018	4,720	25
71-72	<i>Bolivina plicata</i>	10.0	OS-123675	0.4930	0.0013	5,680	20
80-81	<i>Bolivina plicata</i>	7.3	OS-123676	0.4542	0.0012	6,340	20
90-91	<i>Bolivina plicata</i>	6.8	OS-123677	0.4259	0.0015	6,860	30
96-97	<i>Bolivina plicata</i>	6.8	OS-123678	0.3903	0.0013	7,560	25

1413

1414

1415

1416

1417

1418

1419

1420

1421 Table 2. Reservoir age estimation considering the ^{210}Pb age determined with the CRS
 1422 model (McCaffrey and Thomson, 1980) at selected depth sections of the core, as
 1423 compared with ^{14}C ages (y BP) from the marine 13.14 curve (Reimer et al., 2013),
 1424 according to Sabatier et al. (2010).

Core	Depth (cm)	Age from CRS model (AD) ^a	Age years BP ^b	^{14}C age Marine 13.14	^{14}C age BP from foram.	DR
BGGC5	10.5	1828	122	499±24	940±25	441±35
BTCG8	5.5	1908	42	448±23	890±15	442±27

^aAnno Domini

^bBefore present=1950

1425

1426

1427 Table 3. Concentration of elements in the Pachingo wetland sediments, considered as
 1428 lithogenic background for the study area. The values correspond to mean concentrations
 1429 in the surface sediments (0–3 cm).

Element	Metal/Al x 10 ³	s
Ca	686.5	139.3
Fe	591.3	84.5
P	8.6	0.7
Sr	5.7	0.6
Ba	5.6	0.1
Cu	0.258	0.019
Ni	0.174	0.005
U	0.020	0.003
Mo	0.020	0.003
Cd	0.0021	0.0003
Re	0.00004	0.00001

1430

1431

1432

1433

1434

1435

1436

1437

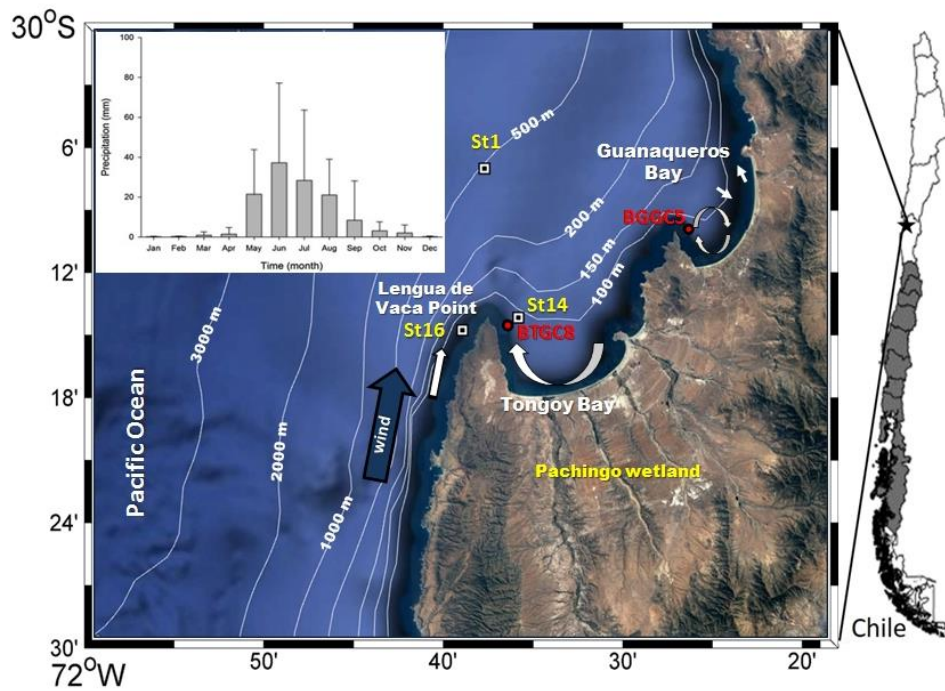
1438 Table 4. Spearman rank order correlations for geochemical data. Significant values

1439 > 0.8 are indicated in bold.

BGGC5																
	Al	P	K	Ca	Mn	Fe	Ni	Cu	Mo	Cd	Re	Sr	U	Ba	Opal	TOC
Al	1.00	-0.62	0.49	-0.48	0.64	0.60	-0.75	0.56	-0.10	-0.73	-0.08	-0.33	0.08	0.49	-0.52	-0.44
P		1.00	-0.31	0.37	-0.45	-0.56	0.56	-0.57	0.01	0.61	-0.11	0.39	-0.12	-0.20	0.49	0.24
K			1.00	-0.24	0.90	0.83	-0.29	0.47	0.28	-0.42	0.33	-0.12	0.50	0.26	-0.25	-0.19
Ca				1.00	-0.47	-0.50	0.44	-0.64	0.23	0.59	0.39	0.92	0.30	-0.60	0.18	0.32
Mn					1.00	0.94	-0.51	0.68	-0.01	-0.68	0.07	-0.32	0.24	0.43	-0.39	-0.31
Fe						1.00	-0.49	0.81	0.03	-0.70	0.11	-0.40	0.23	0.36	-0.37	-0.21
Ni							1.00	-0.51	0.49	0.91	0.35	0.25	0.26	-0.70	0.72	0.64
Cu								1.00	-0.12	-0.71	-0.06	-0.61	0.00	0.31	-0.39	-0.07
Mo									1.00	0.50	0.88	0.10	0.91	-0.48	0.33	0.36
Cd										1.00	0.36	0.42	0.27	-0.67	0.70	0.54
Re											1.00	0.27	0.92	-0.50	0.16	0.38
Sr												1.00	0.24	-0.36	0.05	0.17
U													1.00	-0.39	0.10	0.29
Ba														1.00	-0.30	-0.59
Opal															1.00	0.35
TOC																1.00
BTGC8																
	Al	P	K	Ca	Mn	Fe	Ni	Cu	Mo	Cd	Re	Sr	U	Ba	Opal	TOC
Al	1.00	-0.19	-0.17	-0.37	-0.02	-0.03	-0.39	-0.04	-0.39	0.02	-0.13	-0.58	-0.19	0.07	-0.41	-0.29
P		1.00	0.23	0.00	0.43	0.28	0.58	0.23	0.37	0.13	-0.04	0.30	0.14	-0.14	0.56	0.13
K			1.00	-0.02	0.54	0.41	0.43	0.22	-0.11	0.05	-0.04	0.19	-0.28	0.28	0.26	0.20
Ca				1.00	-0.33	-0.27	0.00	-0.23	0.39	0.01	0.33	0.50	0.47	-0.34	0.20	0.34
Mn					1.00	0.21	0.64	0.01	0.05	0.33	0.15	0.32	-0.02	0.24	0.32	0.00
Fe						1.00	0.13	0.71	-0.40	-0.48	-0.67	-0.37	-0.62	0.13	0.14	0.10
Ni							1.00	0.24	0.56	0.20	0.25	0.64	0.19	-0.16	0.80	0.45
Cu								1.00	-0.25	-0.68	-0.56	-0.22	-0.61	-0.10	0.21	0.37
Mo									1.00	0.45	0.59	0.66	0.69	-0.41	0.58	0.30
Cd										1.00	0.56	0.39	0.52	0.11	0.10	-0.12
Re											1.00	0.53	0.83	-0.16	0.13	0.17
Sr												1.00	0.58	-0.13	0.52	0.23
U													1.00	-0.19	0.21	0.00
Ba														1.00	-0.28	-0.42
Opal															1.00	0.39
TOC																1.00

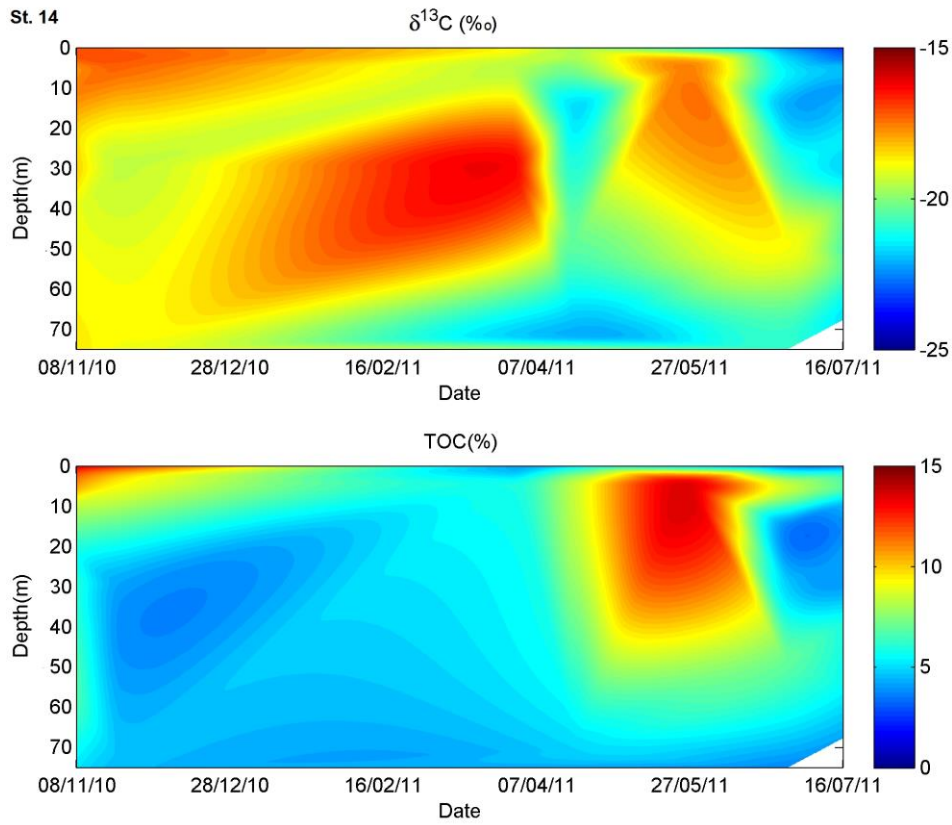
Figures

1440 Figure 1. Study area showing the positions of sampling stations. Sediment cores were
1441 retrieved from Guanaqueros Bay (BGGC5) and Tongoy Bay (BTGC8) at water depths
1442 of 89 and 85 m, respectively. Information of dissolved oxygen in the water column at
1443 St1 and St16 and that of suspended organic particles collected at St14 sampling sites
1444 was gathered in a previous project (INNOVA 07CN13 IXM-150). Monthly
1445 precipitation in mm (bars) (mean \pm SD; Montecinos et al., 2016). Schematic
1446 representation of the circulation in the bays (white arrows) and wind direction (blue
1447 arrow) is indicated, as obtained from Valle-Levinson and Moraga-Opazo (2006) and
1448 Moraga-Opazo et al. (2011).



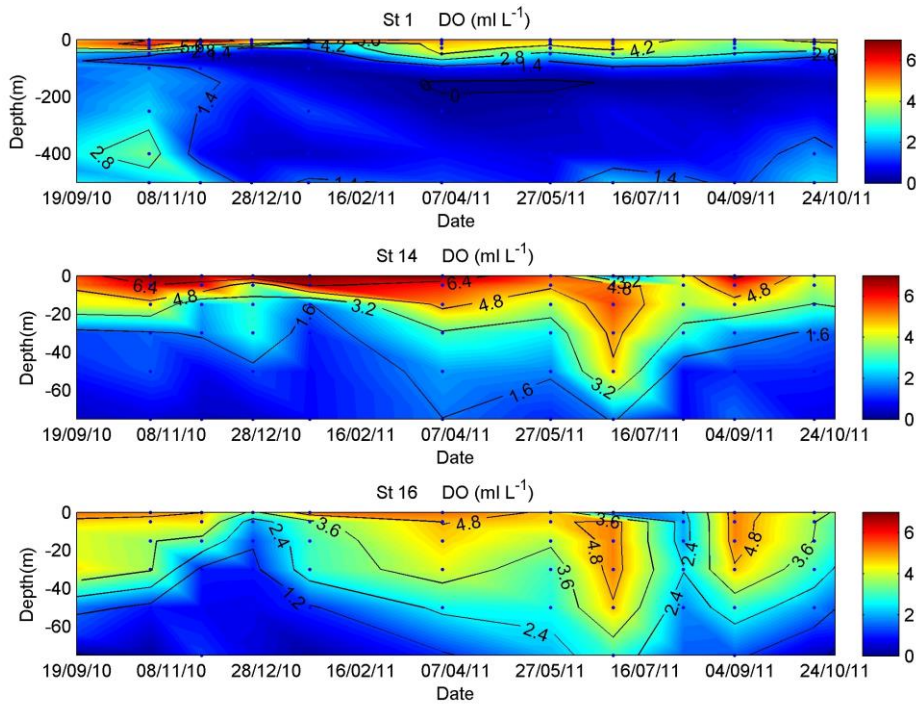
1449
1450
1451
1452
1453
1454

1455 Figure 2. Suspended particulate matter composition (TOC% and $\delta^{13}\text{C}_{\text{org}}$) measured in
1456 the water column between October 2010 and October 2011, at station St14, Tongoy
1457 Bay, Coquimbo (30° S).



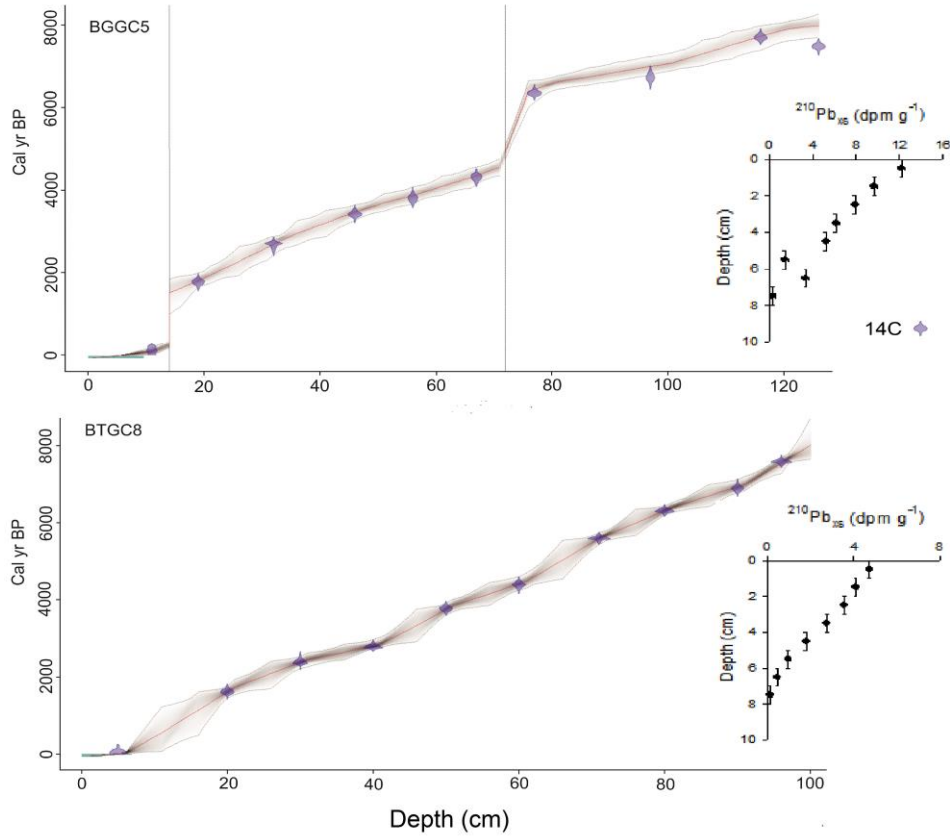
1458
1459
1460
1461
1462
1463
1464
1465
1466
1467
1468
1469

1470 Figure 3. Dissolved oxygen time series in the water column measured between October
1471 2010 and January 2011, at stations St1, St14, and St16 off Tongoy Bay, Coquimbo
1472 (30° S).



1473
1474
1475
1476
1477
1478
1479
1480
1481
1482
1483
1484
1485
1486

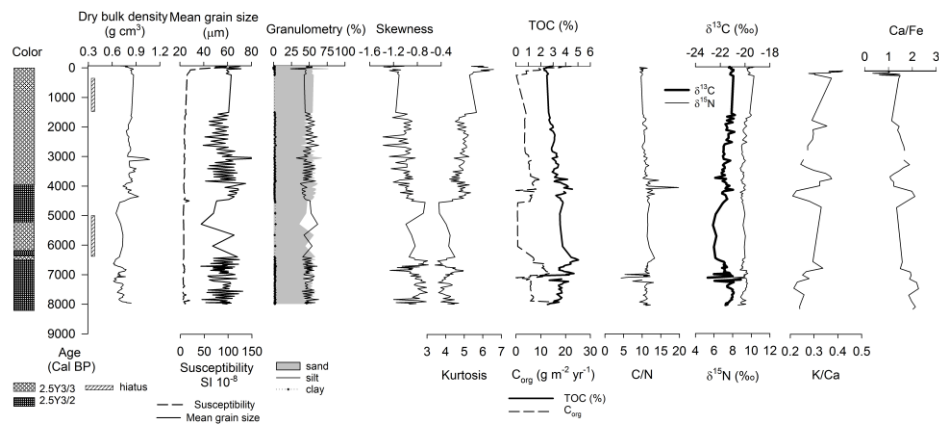
1487 Figure 4. Age model based on ^{14}C -AMS and ^{210}Pb measurements. The timescale was
1488 obtained according to the Bacon age–depth modeling open source software (Blaauw and
1489 Christen, 2011) considering the Marine curve ^{13}C (Reimer et al., 2013).



1490
1491
1492
1493
1494
1495
1496
1497
1498
1499
1500
1501

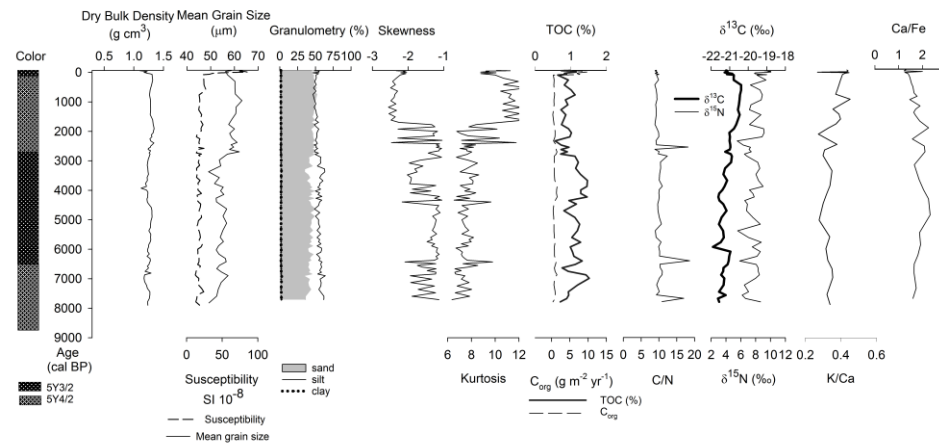
1502 Figure 5. Characterization of sediment cores retrieved from (a) Guanaqueros Bay
 1503 (BGGC5) and (b) Tongoy Bay (BTGC8), where the color (Munsell chart scale)
 1504 represents the depth, dry bulk density, mean grain size, granulometry (% sand, silt,
 1505 and clay), statistical parameters (skewness, kurtosis), organic components (TOC, C/N ratio,
 1506 stable isotopes $\delta^{15}\text{N}$ and $\delta^{13}\text{C}$) and chemical composition (K/Ca, Ca/Fe).

1507 a)



1508

1509 b)



1510

1511

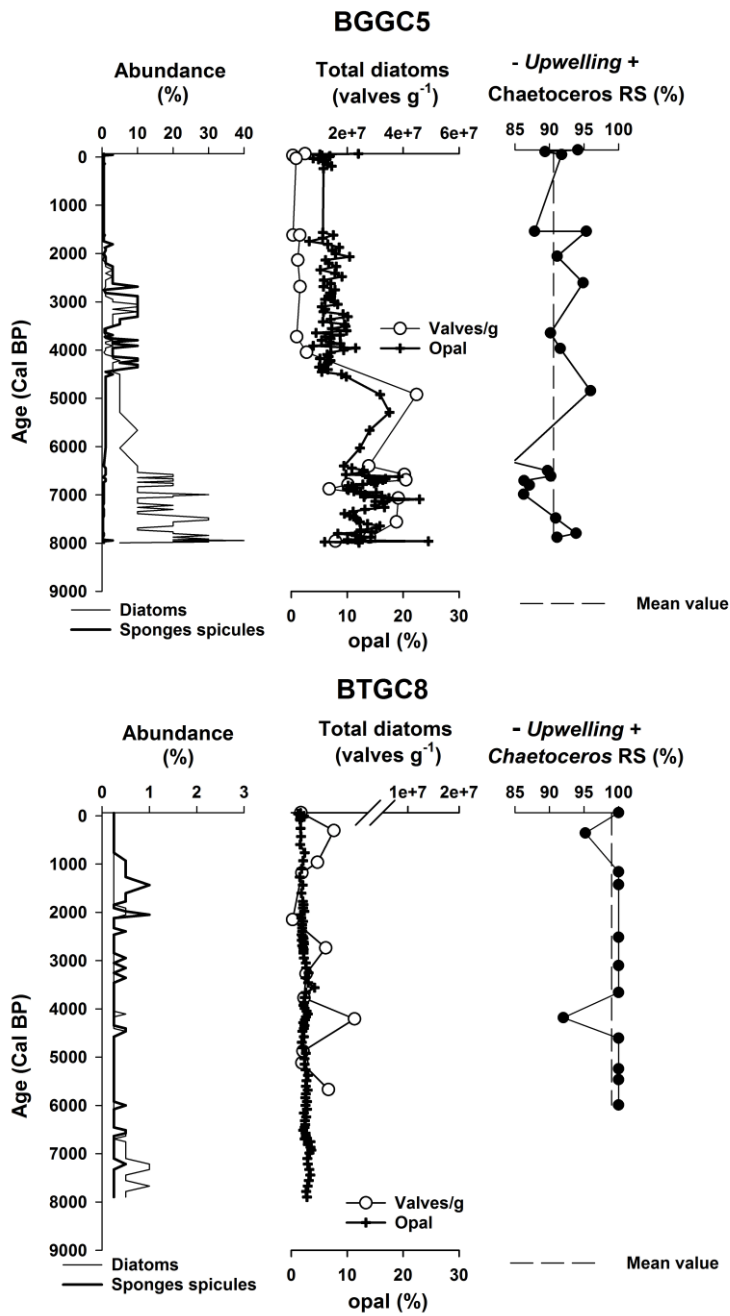
1512

1513

1514

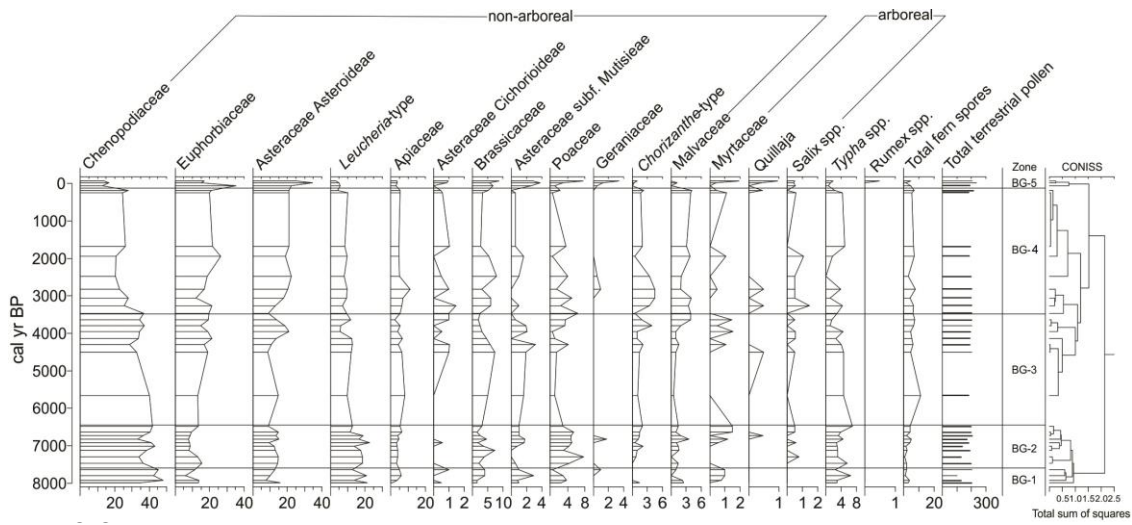
1515

1516 Figure 6. Diatom and sponge spicule relative abundances, total diatom counts (valves g^{-1}) and opal (%), and downcore variations in *Ch. RS* percentages as proxies of upwelling
 1517 intensity in the BGGC5 and BTGC8 cores (Guanaqueros and Tongoy Bay,
 1518 respectively). The medium dashed line represents the average of *Ch. resting* spores for
 1519 respectively).
 1520



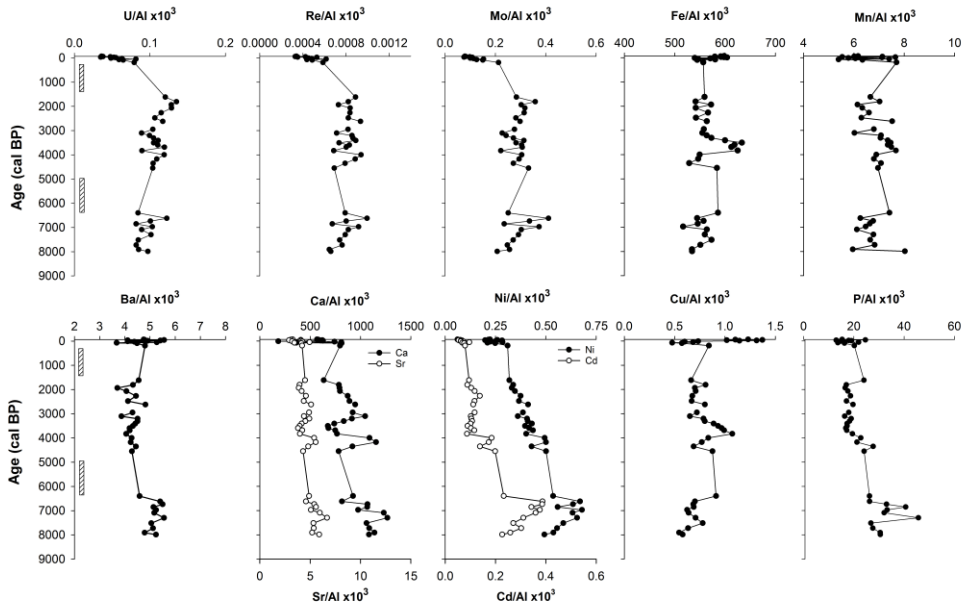
1521

1522 Figure 7. Pollen record in BGGC5 core.

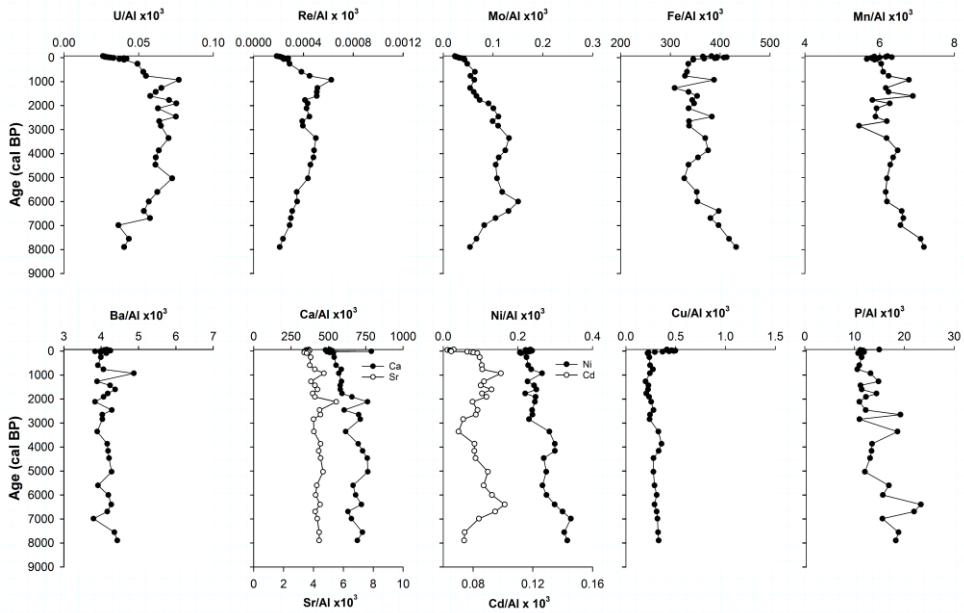


- 1524
- 1525
- 1526
- 1527
- 1528
- 1529
- 1530
- 1531
- 1532
- 1533
- 1534
- 1535
- 1536
- 1537
- 1538
- 1539
- 1540
- 1541
- 1542
- 1543
- 1544

1545 Figure 8. Downcore trace element variations in: (a) Guanaqueros Bay (BGGC5) and (b)
 1546 Tongoy Bay (BTGC8), off Coquimbo (30 °S).
 1547 a)



1548
 1549 b)



1550
 1551

1552 Figure 9. Opal accumulation and authigenic enrichment factor (EF) of trace elements
 1553 calculated for Guanaqueros Bay (BGGC5 core). Lithogenic background was estimated
 1554 from the surface sediments of Pachingo wetland cores (see text). Pollen moisture index
 1555 defined as the normalized ratio between Euphorbiaceae (wet coastal shrub land) and
 1556 Chenopodiaceae (arid scrubland). Positive (negative) values for this index indicate the
 1557 relative expansion (reduction) of coastal vegetation under wetter (drier) conditions. Pb
 1558 and Al distribution at BGGC5 core, representatives of terrigenous input to the bay.
 1559

